(Accepted for Publication in the *IEEE Transactions on Automatic Control* as a Regular Paper)

(Revised Version of 98-276)

Stability Guaranteed Teleoperation: An Adaptive Motion/Force Control Approach

Wen-Hong Zhu Septimiu E. Salcudean

Department of Electrical and Computer Engineering
University of British Columbia
2356 Main Mall, Vancouver, B.C. V6T 1Z4, Canada

Abstract

In this paper, an adaptive motion/force controller is developed for unilateral or bilateral teleoperation systems. The method can be applied in both position and rate control modes, with arbitrary motion or force scaling. No acceleration measurements are required.

Nonlinear rigid-body dynamics of the master and the slave robots are considered. A model of the flexible or rigid environment is incorporated into the dynamics of the slave, while a model of the human operator is incorporated into the dynamics of the master. The master and the slave are subject to independent adaptive motion/force controllers that assume parameter uncertainty bounds. Each parameter is independently updated within its known lower and upper bounds. The states of the master (slave) are sent to the slave (master) as motion/force tracking commands instead of control actions (efforts and/or flows).

Under the modeling assumptions for the human operator and the environment, the proposed teleoperation control scheme is L_2 and L_∞ stable in both free motion and flexible or rigid contact motion, and is robust against time delays. The controlled master-slave system behaves essentially as a linearly damped free-floating mass. If the parameter estimates converge, the environment impedance and the impedance transmitted to the master differ only by a control-parameter dependent mass/damper term. Asymptotic motion (velocity/position) tracking and force tracking with zero steady-state error are achieved. Experimental results are presented in support of the analysis.

Nomenclature

γ	Subscript indicating the properties of the master robot ($\gamma = m$) or the slave robot ($\gamma = s$).
$\Lambda \in R^{6\times 6}$	Diagonal positive-definite control parameter matrix.
$A \in R^{6\times 6}$	Diagonal positive-definite matrix for force feedback, $A = diag\{A_f, A_r\}$.
$A_f \in R^{n_f \times n_f}$	Diagonal positive-definite matrix.
$A_r \in R^{n_r \times n_r}$	Diagonal positive-definite matrix.
$C \in R^{6\times 6}$	Diagonal positive-definite matrix for filters, $C = diag\{C_f, C_r\}$.
$C_f \in R^{n_f \times n_f}$	Diagonal positive-definite matrix.
$C_r \in R^{n_r \times n_r}$	Diagonal positive-definite matrix.
$\kappa_p \in R^{6\times 6}$	Diagonal positive-definite motion scaling matrix.
$\kappa_f \in R^{6\times 6}$	Diagonal positive-definite force scaling matrix.
$\sigma_f \in R$	Selective factor for unilateral flexible environment.
$\sigma_r \in R$	Selective factor for unilateral rigid environment.
$\delta \in R$	Selective factor between position-force mode ($\delta = 1$) and rate-force mode ($\delta = 0$).
$\mathcal{F}_s \in R^6$	Contact force/moment from the slave robot toward the environment, $\mathcal{F}_s = [\mathcal{F}_{sf}^T, \mathcal{F}_{sr}^T]^T$.
$\mathcal{F}_{sf} \in R^{n_f}$	Contact force/moment associated with the flexible environment.
$\mathcal{F}_{sr} \in R^{n_r}$	Contact force/moment associated with the rigid environment.
$\mathcal{F}_m \in R^6$	Contact force/moment from the master robot toward the human operator.
$\mathcal{F}_h^* \in R^6$	Operator Exogenous force/moment.
$\alpha_h \in R$	Upper bound of operator exogenous force.
$\mathcal{P}_s \in R^6$	Position/orientation of the slave robot, $\dot{\mathcal{P}}_s = \mathcal{V}_s$.
$\mathcal{V}_s \in R^6$	Velocity of the slave robot, $\mathcal{V}_s = [\mathcal{V}_{sf}^T, \mathcal{V}_{sr}^T]^T$.
$\mathcal{V}_{sf} \in R^{n_f}$	Velocity associated with the flexible environment.
$\mathcal{V}_{sr} \in R^{n_r}$	Velocity associated with the rigid environment.
$\mathcal{V}_{sd} \in R^6$	Design vector associated with the slave robot, $\mathcal{V}_{sd} = [\mathcal{V}_{sfd}^T, \mathcal{V}_{srd}^T]^T$.
$\mathcal{V}_{srd} \in R^{n_r}$	Design vector associated with the rigid environment.
$\mathcal{P}_m \in R^6$	Position/orientation of the master robot, $\dot{\mathcal{P}}_m = \mathcal{V}_m$.
$\mathcal{V}_m \in R^6$	Velocity of the master robot.
$\mathcal{V}_{md} \in R^6$	Design vector associated with the master robot.
$\mathcal{M}_\gamma \in R^{6\times 6}$	Equivalent inertial matrix of the master or slave robot incorporating operator/environment.
$\mathcal{C}_\gamma \in R^{6\times 6}$	Skew-symmetric matrix.
$\mathcal{G}_\gamma \in R^6$	Equivalent vector.
Θ_γ	Parameter vector of the master or slave robot.
Y_γ	Regressor matrix of the master or slave robot.

I Introduction

Teleoperation system control has been extensively studied, motivated by a large variety of applications [1] ranging from nuclear operations and space exploration [2, 3, 4] to forestry-related tasks [5] and medical applications [6]. Teleoperation can extend a human's reach to a remote site or can

enhance a person's capability to handle both the macro and the micro world.

A typical teleoperation system consists of a master manipulator, a slave manipulator, the human operator, and the operated environment. If only the master motion and/or forces are transmitted to the slave, the teleoperation system is called unilateral. If, in addition, slave motion and/or forces are transmitted to the master, the teleoperation system is called bilateral. Hannaford [7] proposed a two-port teleoperation system model based on circuit theory. Ideal transfer functions are presented and the system deviation from the ideal response is suggested to be the inadequate cancellation of mechanism impedances. The use of observers is proposed to estimate *efforts* and *impedances*. This approach addressed more issues of control architecture than design and no stability or performance measures are given. Kosuge *et al.* [8] proposed an approach to control a single-master and multi-slave manipulator system by using a *virtual internal model*. This approach is based on the complete cancellation of robot dynamics. Goldenberg *et al.* [9] discussed control objectives by specifying hybrid parameters with network theory. Anderson and Spong [10] addressed the time delay issue in maintaining stability for bilateral teleoperation. They used scattering operators to design the controller in such a way that the stability is guaranteed with strictly passive operators and environment. This scheme recently led to a modular controller design applicable to complex robot systems [11]. Although asymptotic stability is ensured [12], no motion/force tracking is provided. Leung *et al.* [13] eliminated the passivity requirement for the operator and the environment, and designed a controller based on H_∞ theory via μ-synthesis. This approach guarantees stability for a pre-specified time-delay margin. Lawrence [14] revealed the conflicting issues between stability and transparency and proposed a unified four-channel control structure. Perfect transparency with ideal kinesthetic feedback was achieved in [15] provided that the master and slave manipulator dynamics are known and their accelerations can be measured. Colgate [16] proposed an impedance shaping control scheme to deal with different impedance and different geometric scales between the task and the human operator. Robust stability criteria were discussed. Lee [17] applied telemonitoring force feedback to address the time delay issue in teleoperation. The trade-off between robustness and performance was explored to achieve optimization. Kazerooni *et al.* [18] and Yan and Salcudean [19] proposed two schemes based on H_∞

optimization which leads to high dimensional matrices with high computational load.

In this paper, a novel teleoperation controller design method is presented based on adaptive motion/force control of the master and slave (see Fig. 1). The approach is applicable to unilateral or bilateral teleoperation in position or rate control modes with arbitrary motion/force scaling. The dynamics of the human operator and the dynamics of the flexible environment are assumed to be second-order mass-damping-stiffness systems with known upper and lower bounds on otherwise unknown parameters. A dynamic model of the human operator is incorporated into the dynamics of the master, while the dynamics of the environment are incorporated into the dynamics of the slave. Each of the master and slave robots are controlled by independent adaptive motion/force controllers. Compared to previous teleoperation designs, this framework has four novel features. First, stability is guaranteed with motion/force tracking, and is robust against time delays. Second, the parameter uncertainties in the systems are well compensated by parameter adaptation and strong feedback control. Third, both rigid and flexible environments are considered. Forth, the full nonlinear dynamics of the master/slave robots which consist of the dynamics of the links and joints, the dynamics of the environment, and the dynamics of the human operator, are taken into account in a *virtual decomposition* based adaptive control design [21], in which each unknown dynamic parameter can be updated independently within its lower and upper bounds. Within a specified frequency range, the master-slave system behaves like a free-floating mass plus a linear damper specified by control parameters, which results in excellent motion tracking and asymptotic force tracking.

This paper is organized as follows: Section II presents the dynamics and adaptive control of the master/slave robots. Bilateral teleoperation design with both position-force and rate-force control is addressed in section III. Section IV presents experimental results. A discussion follows in section V. Finally, conclusions are drawn in sections VI.

II Adaptive Motion/Force Control of Master/Slave Robots

This section presents the adaptive control design of the master robot incorporating a human operator and of the slave robot incorporating a rigid/flexible environment.

A. Dynamics of the Slave Robot Incorporating A Rigid/Flexible Environment

1) The Environment: Without loss of generality, assume that the environment is unilateral, and is flexible in a n_f dimensional space and rigid in a n_r dimensional space, with $n_f + n_r = 6$. For a case in which pure free motion is involved, the free motion can be considered as a special case of flexible contact motion with zero contact force along the free motion subspace.

In general, every environment possesses a certain amount of flexibility. To determine an environment as flexible or rigid is completely dependent on its mechanical impedance. If an environment possesses comparable or lower mechanical impedance than that of the controlled robot, it is considered as a flexible environment. Soft springs and soft tissues are flexible environments. If an environment possesses much higher mechanical impedance than that of the controlled robot, it is considered as a rigid environment. Table mounted aluminum and steel may be considered as rigid environments in most cases.

Two binary selective factors σ_f and σ_r are defined by

$$\sigma_f = \begin{cases} 0 & \text{free motion} \\ 1 & \text{contact with flexible environment} , \end{cases}$$

$$\sigma_r = \begin{cases} 0 & \text{free motion} \\ 1 & \text{contact with rigid constraints} . \end{cases}$$

Let $\mathcal{F}_s = [\mathcal{F}_{sf}^T \ \mathcal{F}_{sr}^T]^T \in R^6$ be the contact force from the slave robot toward the flexible/rigid environment, expressed in a special task frame Ψ, and let $\mathcal{V}_s = [\mathcal{V}_{sf}^T \ \mathcal{V}_{sr}^T]^T \in R^6$ be the velocity expressed in the same task frame Ψ, where $\mathcal{F}_{sf} \in R^{n_f}$ and $\mathcal{V}_{sf} \in R^{n_f}$ are associated with the flexible contact, and $\mathcal{F}_{sr} \in R^{n_r}$ and $\mathcal{V}_{sr} \in R^{n_r}$ are associated with the rigid contact. The rigid contact dynamics is

$$\mathcal{V}_{sr} = (1 - \sigma_r) \ \mathcal{V}_{sr} , \tag{1}$$

$$\mathcal{F}_{sr} = \sigma_r \ \mathcal{F}_{sr} ; \tag{2}$$

and the flexible contact dynamics is

$$\sigma_f \ [M_f \ \ddot{\mathcal{X}}_{sf} + D_f \ \dot{\mathcal{X}}_{sf} + \delta \ K_f \ \mathcal{X}_{sf} + (1 - \delta) \ \varphi_f] = \mathcal{F}_{sf} , \tag{3}$$

$$\dot{\mathcal{X}}_{sf} = \sigma_f \ \mathcal{V}_{sf} , \tag{4}$$

where

$$\delta \triangleq \begin{cases} 1 & \text{position} - \text{force control mode} \\ 0 & \text{rate} - \text{force control mode} \end{cases}$$

is a binary selective factor between position-force control mode and rate-force control mode, $\varphi_f \in R^{n_f} \cap L_\infty$ is a bounded vector with known form and unknown parameters, M_f, D_f, and K_f are $n_f \times n_f$ constant, time-invariant, symmetric, and positive-definite matrices associated with the inertia, the damping, and the stiffness of the flexible environment, respectively, and $\mathcal{X}_{sf}$ denotes the deformation of the flexible environment, i.e. the error between the current position/orientation and the position/orientation at contact.

Remark 2.1: The special task frame Ψ is completely application oriented. The choice of this frame with special partition of flexible/rigid contacts requires a priori knowledge of what the operator is attempting to achieve.

Remark 2.2: In modeling the dynamics of the flexible environment, only second-order linear time-invariant (LTI) models are considered for simplicity. The extension of this model to a more general case requires further research.

Remark 2.3: Euler parameter (quaternion expression) is used to represent all orientations in $SO(3)$ throughout this paper. For each quaternion expression, the unique singularity point corresponding to a rotation of π from the reference orientation is assumed not to be reached. This means that for large changes in orientation, the reference orientation should be changed by rate-force control.

Remark 2.4: The model (3) is able to incorporate pure free motion as long as the corresponding elements of M_f, D_f, K_f, and φ_f are set to zero, while still maintaining symmetric positive-definite property in the remaining flexible contact subspace.

Remark 2.5: In the model (3), no stiffness term is assumed when rate-force control is used. This is true for some applications such as soil excavation where the position-dependent resistant force in the sliding direction can be bounded. For other applications, if a stiffness term is necessarily involved with rate-force control and the slave working range is limited, then this stiffness term is bounded and can be included in φ_f.

2) The Slave Robot: A 6×6 reordering matrix $[S_f \ S_r]$ is formed such that

$$\left[\begin{array}{cc} S_f & S_r \end{array} \right]^{-1} = \left[\begin{array}{c} S_f^T \\ S_r^T \end{array} \right] ,$$

where $S_f \in R^{6 \times n_f}$ and $S_r \in R^{6 \times n_r}$ contain unit, orthogonal, and constant vectors that span the flexible contact subspace and the rigid contact subspace, respectively.

A frame O is located at the contact point between the environment and the slave robot, and is fixed to the slave robot. The force/moment and linear/angular velocity of frame O and expressed in frame O [21] can be written as

$$^{O}F = T_o^{-T} \left[\begin{array}{cc} S_f & S_r \end{array} \right] \left[\begin{array}{c} \sigma_f \ \mathcal{F}_{sf} \\ \sigma_r \ \mathcal{F}_{sr} \end{array} \right] , \tag{5}$$

$$^{O}V = T_o \left[\begin{array}{cc} S_f & S_r \end{array} \right] \left[\begin{array}{c} \mathcal{V}_f \\ (1 - \sigma_r) \ \mathcal{V}_r \end{array} \right] , \tag{6}$$

where $T_o \in R^{6 \times 6}$ is an invertible transformation matrix, e.g. the right-low 3×3 sub-matrix may represent the transformation between angular velocity and the time-derivative of quaternion expression, and remains full-rank as long as the unique singularity point is not reached.

Based on the concept of *virtual decomposition* [21], only the dynamics of the links and joints are required to represent the dynamics of a robot. Assume that the slave robot is a six-joint robot. Joint j, $j = 1, 2, \cdots, 6$, connects link $j-1$ with link j. Link 0 is connected to the base and link 6 is connected to the end-effector. Six auxiliary frames L_j, $j = 1, 2, \cdots, 6$, are each fixed to link j with their z axis coincident with the jth joint.

The velocity transformation equation within the manipulator is

$$^{L_j}V = ^{L_{j-1}}U_{L_j}^T \ ^{L_{j-1}}V + Z_j \ \dot{q}_j , \tag{7}$$

where $q_j \in R$ denotes the displacement of the jth joint, $Z_j = [0 \ 0 \ 1 \ 0 \ 0 \ 0]^T$ for a prismatic joint and $Z_j = [0 \ 0 \ 0 \ 0 \ 0 \ 1]^T$ for a revolute joint, $^{L_{j-1}}U_{L_j} \in R^{6 \times 6}$ denotes a force/moment transformation matrix which transforms a force/moment measured and expressed in frame L_j to that measured and expressed in frame L_{j-1}, and $^{L_j}V \in R^6$ denotes a generalized linear/angular velocity of frame L_j and expressed in frame L_j. By setting $\dot{q}_j = 0$, (7) gives the velocity transformation within a rigid body.

The dynamics of joint j is

$$\underline{\tau}_j \triangleq I_j^* \ \ddot{q}_j + \xi_j(t) + d_j = \tau_j - Z_j^T \ {}^{L_j}F \ , \tag{8}$$

where $I_j^* \in R$ is the equivalent rotational inertia, $\xi_j(t) \in R$ is the frictional force/torque, and $d_j \in R$ denotes a constant uncertainty, $\tau_j \in R$ is the joint control force/torque, and ${}^{L_j}F \in R^6$ denotes the exerting force/moment from link $j-1$ toward link j, measured and expressed in frame L_j.

The dynamics of link j can be written as

$$M_{L_j} \ \frac{d}{dt}({}^{L_j}V) + C_{L_j} \ {}^{L_j}V + G_{L_j} = {}^{L_j}\underline{F} \ , \tag{9}$$

where $M_{L_j} \in R^{6\times 6}$ is constant, symmetric, and positive-definite, $C_{L_j} \in R^{6\times 6}$ is skew-symmetric, $G_{L_j} \in R^6$ is a vector [21], ${}^{L_j}\underline{F}$ denotes the net force/moment of link j and is governed by

$${}^{L_j}\underline{F} = {}^{L_j}F - {}^{L_j}U_{L_{j+1}} \ {}^{L_{j+1}}F \tag{10}$$

with ${}^{L_7}F = {}^{O}F$.

In view of (1)-(10), the dynamic model of the slave robot incorporating the rigid/flexible environment can be written as

$$(\mathcal{T}_s^T \ \mathcal{M}_s \ \mathcal{T}_s) \ \dot{\mathcal{V}}_s + (\mathcal{T}_s^T \ \mathcal{C}_s \ \mathcal{T}_s + \mathcal{T}_s^T \ \mathcal{M}_s \ \dot{\mathcal{T}}_s) \ \mathcal{V}_s + \mathcal{T}_s^T \ \mathcal{G}_s = T_s^{-1} \ \tau_s - \begin{bmatrix} 0 \\ \sigma_r \ \mathcal{F}_{sr} \end{bmatrix} \ , \tag{11}$$

where

$$\begin{aligned}
\mathcal{V}_s &= \begin{bmatrix} \mathcal{V}_{sf}^T & (1-\sigma_r) \ \mathcal{V}_{sr}^T \end{bmatrix}^T \ , \\
\tau_s &= [\tau_1, \cdots, \tau_j, \cdots, \tau_6]^T \ , \\
\mathcal{M}_s &= diag\{\mathcal{M}^*, \sigma_f \ M_f\} \ , \\
\mathcal{C}_s &= diag\{\mathcal{C}^*, 0\} \ , \\
\mathcal{G}_s &= \left[\mathcal{G}^{*T}, [D_f \ \dot{\mathcal{X}}_{sf} + \delta \ K_f \ \mathcal{X}_{sf} + (1-\delta) \ \varphi_f]^T\right]^T \ , \\
\mathcal{T}_s &= \begin{bmatrix} \Phi \ J^{-1} \ T_o \begin{bmatrix} S_f & S_r \end{bmatrix} \\ \begin{bmatrix} I_{n_f} & 0_{n_f \times n_r} \end{bmatrix} \end{bmatrix} \ , \\
T_s &= J^T \ T_o^{-T} \begin{bmatrix} S_f & S_r \end{bmatrix} \ ,
\end{aligned}$$

$$
\begin{aligned}
\mathcal{M}^* &= diag\{I_1^*, \cdots, I_6^*, M_{L_1}, \cdots, M_{L_6}\} \,, \\
\mathcal{C}^* &= diag\{0, \cdots, 0, C_{L_1}, \cdots, C_{L_6}\} \,, \\
\mathcal{G}^* &= [(\xi_1(t) + d_1), \cdots, (\xi_6(t) + d_6), G_{L_1}^T, \cdots, G_{L_6}^T]^T \,, \\
J &= \left[\begin{array}{cccc} {}^{L_1}U_O^T \; Z_1 & {}^{L_2}U_O^T \; Z_2 & \cdots & {}^{L_6}U_O^T \; Z_6 \end{array} \right] \,, \\
\Phi &= \left[\begin{array}{cccc} I_6 & & & \\ Z_1 & & & \\ {}^{L_1}U_{L_2}^T \; Z_1 & Z_2 & & \\ \vdots & \ddots & \ddots & \\ {}^{L_1}U_{L_6}^T \; Z_1 & {}^{L_2}U_{L_6}^T \; Z_2 & \cdots & Z_6 \end{array} \right] .
\end{aligned}
$$

A detailed procedure for obtaining (11) is given in Appendix A.

B. Dynamics of the Master Robot Incorporating the Human Operator

1) The Human Operator: Based on the research in [22, 23], the following two-order LTI model is used for the operator.

$$M_h \; \ddot{\mathcal{X}}_h + D_h \; \dot{\mathcal{X}}_h + K_h \; \mathcal{X}_h = \mathcal{F}_m - \mathcal{F}_h^* \,, \tag{12}$$

where M_h, D_h, and K_h are three 6×6 constant, time-invariant, symmetric, and positive-definite matrices associated with the inertia, the damping, and the stiffness of the human operator, $\mathcal{F}_m \in R^6$ is the reaction force/moment from the master robot toward the human hand, $\mathcal{F}_h^* \in R^6$ denotes the exogenous force/moment generated by the operator, subject to

$$\|\mathcal{F}_h^*\|_\infty \leq \alpha_h < +\infty \tag{13}$$

where α_h is a positive constant, and $\mathcal{X}_h = [x_h^T \; \mu_h^T]^T \in R^6$ denotes the position/orientation of the human operator, where $x_h \in R^3$ is the linear position and $\mu_h \in R^3$ is the vector part of a quaternion expression $[\xi_h, \; \mu_h^T]^T \in R^4$ between the current operator hand orientation and the reference orientation.

Remark 2.6: The dynamics of a real human operator is very complicated, is posture-dependent, time-dependent, and subject-dependent. The LTI model (12) is only an approximation at certain operation points within certain parameter ranges. Further research will take into account the adaptive properties of the human operator with respect to object control dynamics.

Remark 2.7: The quaternion expression is used to express the operator hand orientation. Rotation of π will not happen in most cases. Therefore, this quaternion expression is assumed to be singularity free.

Assume that a frame Υ is fixed to the handle of the master robot. The velocity transformation from $\dot{\mathcal{X}}_h$ to ${}^{\Upsilon}V$ is

$$T_h = \begin{bmatrix} {}^{\Upsilon}R_I & 0 \\ 0 & \left[\frac{1}{2}\left[\xi_h\ I_3 - (\mu_h\times)\right]\right]^{-1} \end{bmatrix},$$

where ${}^{\Upsilon}V \in R^6$ denotes a generalized linear/angular velocity of frame Υ, expressed in frame Υ, and ${}^{\Upsilon}R_I \in R^{3\times 3}$ is a rotational matrix which transforms a vector expressed in the inertial frame to that expressed in frame Υ. Matrix $T_h \in R^{6\times 6}$ remains full-rank as long as $\xi_h \neq 0$.

2) The Master Robot: By setting

$$\mathcal{P}_m = \mathcal{X}_h\ ,\quad \mathcal{V}_m = \dot{\mathcal{X}}_h\ ,\quad \dot{\mathcal{V}}_m = \ddot{\mathcal{X}}_h\ , \tag{14}$$

and following an approach similar to that leads to (11), the dynamic equation of the master robot incorporating the human operator can be obtained as

$$(\mathcal{T}_m^T\ \mathcal{M}_m\ \mathcal{T}_m)\ \dot{\mathcal{V}}_m + (\mathcal{T}_m^T\ \mathcal{C}_m\ \mathcal{T}_m + \mathcal{T}_m^T\ \mathcal{M}_m\ \dot{\mathcal{T}}_m)\ \mathcal{V}_m + \mathcal{T}_m^T\ \mathcal{G}_m = T_m^{-1}\ \tau_m - \mathcal{F}_h^*\ , \tag{15}$$

where

$$\begin{aligned}
\mathcal{M}_m &= diag\{\mathcal{M}^*, M_h\}\ , \\
\mathcal{C}_m &= diag\{\mathcal{C}^*, 0\}\ , \\
\mathcal{G}_m &= \left[\mathcal{G}^{*T}, [D_h\ \dot{\mathcal{X}}_h + K_h\ \mathcal{X}_h]^T\right]^T\ , \\
\mathcal{T}_m &= \begin{bmatrix} \Phi\ J^{-1}\ T_h \\ I_6 \end{bmatrix}, \\
T_m &= J^T\ T_h^{-T}\ ,
\end{aligned}$$

$\tau_m \in R^6$ is the control vector, $\mathcal{M}^*$, $\mathcal{C}^*$, $\mathcal{G}^*$, J, and Φ have the similar forms as these in (11), except frame Υ is substituted for frame O.

Remark 2.8: It is clear from (11) and (15) that the dynamics of the flexible environment is incorporated into the dynamics of the slave robot and the dynamics of the human operator is incorporated into the dynamics of the master robot.

C. Adaptive Control Design

The control laws for both the slave robot (11) and the master robot (15) are designed as

$$\tau_s = T_s \left[\mathcal{T}_s^T \mathcal{Y}_s \hat{\Theta}_s + \begin{bmatrix} 0 \\ \sigma_r A_r^{-1} (C_r^{-1} \dot{\mathcal{V}}_{srd} + \mathcal{V}_{srd}) \end{bmatrix} + \mathcal{K}_s (\mathcal{V}_{sd} - \mathcal{V}_s - A \tilde{\mathcal{F}}_s) \right] , \quad (16)$$

$$\tau_m = T_m \left[\mathcal{T}_m^T \mathcal{Y}_m \hat{\Theta}_m + \mathcal{K}_m (\mathcal{V}_{md} - \mathcal{V}_m - A \tilde{\mathcal{F}}_m) + \alpha_h \, \text{sign}(\mathcal{V}_{md} - \mathcal{V}_m - A \tilde{\mathcal{F}}_m) \right] , \quad (17)$$

where $\mathcal{V}_{sd} = [\mathcal{V}_{sfd}^T, \mathcal{V}_{srd}^T]^T \in R^6$ with $\mathcal{V}_{sfd} \in R^{n_f}$ and $\mathcal{V}_{srd} \in R^{n_r}$, and $\mathcal{V}_{md} \in R^6$ are two command vectors, $\mathcal{K}_\gamma \in R^{6\times 6}$, $\gamma = \{s, m\}$, is a positive-definite feedback gain matrix, $A = diag\{A_f, A_r\} \in R^{6\times 6}$ is a diagonal positive-definite matrix with small elements, where $A_f \in R^{n_f}$ and $A_r \in R^{n_r}$, $\tilde{\mathcal{F}}_\gamma \in R^6$ denotes a filtered contact force governed by

$$\dot{\tilde{\mathcal{F}}}_\gamma + C \tilde{\mathcal{F}}_\gamma = C \mathcal{F}_\gamma , \quad (18)$$

where $C = diag\{C_f, C_r\} \in R^{6\times 6}$ is a diagonal positive-definite matrix with $C_f \in R^{n_f}$ and $C_r \in R^{n_r}$, $\hat{\Theta}_\gamma$ denotes the estimate of Θ_γ which contains all constant dynamic parameters of the slave or master robot, and $\mathcal{Y}_\gamma$ is a regressor matrix defined by

$$\mathcal{Y}_\gamma \Theta_\gamma = \mathcal{M}_\gamma \frac{d}{dt}[\mathcal{T}_\gamma (\mathcal{V}_{\gamma d} - A \tilde{\mathcal{F}}_\gamma)] + \mathcal{C}_\gamma \mathcal{T}_\gamma (\mathcal{V}_{\gamma d} - A \tilde{\mathcal{F}}_\gamma) + \mathcal{G}_\gamma . \quad (19)$$

The block diagonal property of $\mathcal{M}_\gamma$ and $\mathcal{C}_\gamma$ makes $\mathcal{Y}_\gamma$ block diagonal. It follows that

$$\mathcal{Y}_\gamma \Theta_\gamma = \left[(\mathcal{Y}_{\gamma 1} \Theta_{\gamma 1})^T, \cdots, (\mathcal{Y}_{\gamma k} \Theta_{\gamma k})^T, \cdots \right]^T , \quad (20)$$

where $\mathcal{Y}_{\gamma k} \Theta_{\gamma k}$ corresponds to the kth subsystem which may be a rigid link (9), a joint (8), the environment (3), or the human operator (12). The block diagonal structure of $\mathcal{Y}_\gamma \Theta_\gamma$ allows parallel calculations to take place in controller implementations.

Remark 2.9: The control laws (16) and (17) are typically model-based feedforward compensation plus feedback control. The design philosophy is similar to the Slotine and Li controller [24]. The first two terms in the right hand side of (16) and the first term in the right hand side of (17) are feedforward compensation terms. The remaining terms in the right hand sides of (16) and (17) are feedback correction terms.

Remark 2.10: The introduction of force signals into velocity feedback can be found in previous publications [25, 26]. However, force signals are used differently in this paper. First, a filtered force instead of the force integral is used; and second, a small gain matrix A is used as opposed to [25, 26]. As will be seen below, using a small gain matrix A is a key point in achieving a stability guaranteed design.

Remark 2.11: In control law (16), the desired contact force in rigid constraint space is taken as a feedforward term enabled by the rigid contact binary factor σ_r. The value of σ_r can be determined by the relationship between the velocity and the contact force, since in rigid contact there is zero velocity with a considerable amount of force.

The parameter adaptation for both the slave and master robots is proposed as

$$\dot{\hat{\Theta}}_{\gamma i} = \rho_{\gamma i}\ \kappa_{\gamma i}\ s_{\gamma i}\ , \tag{21}$$

$$s_{\gamma i} = \mathcal{Y}_{\gamma i}^T\ \mathcal{T}_\gamma\ (\mathcal{V}_{\gamma d} - \mathcal{V}_\gamma - A\ \tilde{\mathcal{F}}_\gamma)$$

$$\kappa_{\gamma i} = \begin{cases} 0 & \hat{\Theta}_{\gamma i} \le \Theta_{\gamma i}^- \text{ and } s_{\gamma i} \le 0 \\ 0 & \hat{\Theta}_{\gamma i} \ge \Theta_{\gamma i}^+ \text{ and } s_{\gamma i} \ge 0 \\ 1 & \text{otherwise} \end{cases}$$

where the subscript γi is assigned to the ith parameter of either the salve ($\gamma = s$) or the master ($\gamma = m$) robot, $\rho_{\gamma i} > 0$ is the update gain for the ith parameter, $\mathcal{Y}_{\gamma i}$ denotes the ith column of $\mathcal{Y}_\gamma$, and $\Theta_{\gamma i}^-$ and $\Theta_{\gamma i}^+$ denote the lower and upper bounds of the ith parameter $\Theta_{\gamma i}$. By assuming $\Theta_{\gamma i} \in [\Theta_{\gamma i}^-, \Theta_{\gamma i}^+]$, it is easy to check from (21) that

$$(\Theta_{\gamma i} - \hat{\Theta}_{\gamma i})\ (s_{\gamma i} - \dot{\hat{\Theta}}_\gamma/\rho_{\gamma i}) = (\Theta_{\gamma i} - \hat{\Theta}_{\gamma i})\ s_{\gamma i}\ (1 - \kappa_{\gamma i}) \le 0\ . \tag{22}$$

A simple example of applying (16), (19) and (21) is given in Appendix B.

Remark 2.12: Parameter adaptation (21) can be performed with respect to each parameter independently. Each parameter is assigned a pair of lower and upper bounds $\Theta_{\gamma i}^-$ and $\Theta_{\gamma i}^+$, which can prevent the parameter estimate from drifting. A large difference between the lower and upper bounds means a large uncertainty of the parameter. For a known parameter, of course, its lower bound is exactly equal to its upper bound.

Calculations of (16), (17), and (21) involve three steps as follows:

1) *Step 1*: Calculate $\mathcal{T}_\gamma\ \mathcal{V}_\gamma$ and $\mathcal{T}_\gamma\ (\mathcal{V}_{\gamma d} - A\ \tilde{\mathcal{F}}_\gamma)$. This step is performed recursively.

2) *Step 2*: Calculate $\mathcal{Y}_\gamma\ \hat{\Theta}_\gamma$ in (20) and $\dot{\hat{\Theta}}_\gamma$ in (21). This step is performed in parallel because of the block diagonal structure of $\mathcal{M}_\gamma$ and $\mathcal{C}_\gamma$, and in turn the block diagonal structure of $\mathcal{Y}_\gamma\ \hat{\Theta}_\gamma$.

3) *Step 3*: Calculate (16) and (17). A corresponding recursive calculation is required.

D. Stability

Substituting (16) into (11), and (17) into (15) and using (19) yield

$$\begin{aligned}
&\mathcal{T}_s^T\ \mathcal{M}_s\ \frac{d}{dt}\left[\mathcal{T}_s\ (\mathcal{V}_{sd} - \mathcal{V}_s - A\ \tilde{\mathcal{F}}_s)\right] \\
&= -(\mathcal{T}_s^T\ \mathcal{C}_s\ \mathcal{T}_s + \mathcal{K}_s)\ (\mathcal{V}_{sd} - \mathcal{V}_s - A\ \tilde{\mathcal{F}}_s) - \begin{bmatrix} 0 \\ \sigma_r\ [A_r^{-1}\ (C_r^{-1}\ \dot{\mathcal{V}}_{srd} + \mathcal{V}_{srd}) - \mathcal{F}_{sr}] \end{bmatrix} \\
&\quad + \mathcal{T}_s^T\ \mathcal{Y}_s\ (\Theta_s - \hat{\Theta}_s)\ , \qquad (23) \\
&\mathcal{T}_m^T\ \mathcal{M}_m\ \frac{d}{dt}\left[\mathcal{T}_m\ (\mathcal{V}_{md} - \mathcal{V}_m - A\ \tilde{\mathcal{F}}_m)\right] \\
&= -(\mathcal{T}_m^T\ \mathcal{C}_m\ \mathcal{T}_m + \mathcal{K}_m)\ (\mathcal{V}_{md} - \mathcal{V}_m - A\ \tilde{\mathcal{F}}_m) + [\mathcal{F}_h^* - \alpha_h\ \mathrm{sign}(\mathcal{V}_{md} - \mathcal{V}_m - A\ \tilde{\mathcal{F}}_m)] \\
&\quad + \mathcal{T}_m^T\ \mathcal{Y}_m\ (\Theta_m - \hat{\Theta}_m)\ . \qquad (24)
\end{aligned}$$

Two non-negative functions are chosen as

$$\begin{aligned}
V_s &= \frac{1}{2}\Big[(\mathcal{V}_{sd} - \mathcal{V}_s - A\ \tilde{\mathcal{F}}_s)^T\ \mathcal{T}_s^T\ \mathcal{M}_s\ \mathcal{T}_s\ (\mathcal{V}_{sd} - \mathcal{V}_s - A\ \tilde{\mathcal{F}}_s) \\
&\quad + \sigma_r\ (\mathcal{V}_{srd} - A_r\ \tilde{\mathcal{F}}_{sr})^T\ (A_r\ C_r)^{-1}\ (\mathcal{V}_{srd} - A_r\ \tilde{\mathcal{F}}_{sr}) + \sum_i (\Theta_{si} - \hat{\Theta}_{si})^2/\rho_{si}\Big]\ , \qquad (25) \\
V_m &= \frac{1}{2}\Big[(\mathcal{V}_{md} - \mathcal{V}_m - A\ \tilde{\mathcal{F}}_m)^T\ \mathcal{T}_m^T\ \mathcal{M}_m\ \mathcal{T}_m\ (\mathcal{V}_{md} - \mathcal{V}_m - A\ \tilde{\mathcal{F}}_m) \\
&\quad + \sum_i (\Theta_{mi} - \hat{\Theta}_{mi})^2/\rho_{mi}\Big]\ . \qquad (26)
\end{aligned}$$

For constant σ_f and σ_r, the time-derivatives of (25) and (26) are obtained below in (27) and (28), using (23), (24), (18), (22), and the fact that $\mathcal{C}_\gamma$ is skew-symmetric.

$$\begin{aligned}
\dot{V}_s &\leq -(\mathcal{V}_{sd} - \mathcal{V}_s - A\ \tilde{\mathcal{F}}_s)^T\ \mathcal{K}_s\ (\mathcal{V}_{sd} - \mathcal{V}_s - A\ \tilde{\mathcal{F}}_s) \\
&\quad - \sigma_r\ (\mathcal{V}_{srd} - A_r\ \tilde{\mathcal{F}}_{sr})^T\ (A_r^{-1})\ (\mathcal{V}_{srd} - A_r\ \tilde{\mathcal{F}}_{sr})\ , \qquad (27) \\
\dot{V}_m &\leq -(\mathcal{V}_{md} - \mathcal{V}_m - A\ \tilde{\mathcal{F}}_m)^T\ \mathcal{K}_m\ (\mathcal{V}_{md} - \mathcal{V}_m - A\ \tilde{\mathcal{F}}_m)\ . \qquad (28)
\end{aligned}$$

Theorem 1: Consider a slave robot incorporating a rigid/flexible environment (11) and a master robot incorporating a human operator (15) subject to control (16) and (17), respectively, under the parameter adaptation (21). It follows that

$$\rho_s \triangleq \mathcal{V}_{sd} - \mathcal{V}_s - A\,\tilde{\mathcal{F}}_s \in L_2 \bigcap L_\infty\,, \tag{29}$$

$$\rho_m \triangleq \mathcal{V}_{md} - \mathcal{V}_m - A\,\tilde{\mathcal{F}}_m \in L_2 \bigcap L_\infty \tag{30}$$

for constant σ_f and σ_r.

Proof: In view of (25)-(28), it follows that $V_s \geq 0$, $V_m \geq 0$, $\dot{V}_s \leq 0$, and $\dot{V}_m \leq 0$ for constant σ_f and σ_r. This implies that $\rho_s \in L_\infty$ and $\rho_m \in L_\infty$. Furthermore, integrating (27) and (28) yields $\rho_s \in L_2$ and $\rho_m \in L_2$.

$\nabla\ \nabla\ \nabla$

Remark 2.13: Note that (29) is valid only when σ_f (σ_f is involved in $\mathcal{M}_s$) and σ_r are constant, either *one* or *zero*. When transition phases are considered, V_s can be uniformly continuous, i.e. $\dot{V}_s \in L_\infty$, only when the flexible environment has zero mass ($M_f = 0$ in (3)) and $n_r = 0$. In other cases of rigid contact (where the velocity jumps to zero at contact) and flexible contact with non-zero environment mass (where the mass collision happens, which also leads to velocity jump), infinite acceleration occur. Therefore $\dot{V}_s \in L_\infty$ may not hold. The stability analysis for transition phases of rigid contact and of non-zero mass collisions remains an issue for further research.

III Teleoperation

Since both the slave robot incorporating the environment and the master robot incorporating the operator are subject to independent adaptive motion/force control, the teleoperation design is greatly simplified and involves specifying two design vectors $\mathcal{V}_{sd}$ and $\mathcal{V}_{md}$. In this section, both unilateral teleoperation where only $\mathcal{V}_{sd}$ is specified and bilateral teleoperation where both $\mathcal{V}_{sd}$ and $\mathcal{V}_{md}$ are specified are addressed.

A. Unilateral Teleoperation

In unilateral teleoperation, commands only flow from the master to the slave. There is no force information feedback to the master. The only design vector $\mathcal{V}_{sd}$ is obtained from

$$\dot{\mathcal{V}}_{sd} + C\ \mathcal{V}_{sd} = C\ R(t)\ , \tag{31}$$

where $R(t) \in L_\infty$ denotes the command from the master robot.

Lemma 1: Consider an equation $\dot{x} + c\ x = u$, where $c > 0$ is a positive constant, and x is a differentiable function. If $u \in L_\infty$, then $\dot{x} \in L_\infty$ and $x \in L_\infty$; and if $u \in L_2$, then $\dot{x} \in L_2$ and $x \in L_2$.

$\nabla\ \nabla\ \nabla$

Lemma 2: Consider an ordinary differential equation

$$M\ \ddot{X} + D\ \dot{X} + K\ X = U\ ,$$

where M, D, and K are $n \times n$, $n \geq 1$, time-invariant symmetric positive-definite matrices. If $U \in L_\infty^n$, then $X \in L_\infty^n$, $\dot{X} \in L_\infty^n$, and $\ddot{X} \in L_\infty^n$.

$\nabla\ \nabla\ \nabla$

In view of (31) and Lemma 1, it follows that $\dot{\mathcal{V}}_{sd} \in L_\infty$ and $\mathcal{V}_{sd} \in L_\infty$. From (29), (1)-(4), (18), and Lemma 2, it follows that $\mathcal{V}_{sr} \in L_\infty$, $\dot{\tilde{\mathcal{V}}}_{sf} \in L_\infty$, $\tilde{\mathcal{V}}_{sf} \in L_\infty$, $\tilde{\mathcal{X}}_{sf} \in L_\infty$, and $\tilde{\mathcal{F}}_s \in L_\infty$, where $\tilde{Q}_f$, $Q_f = \{\mathcal{V}_{sf}, \mathcal{X}_{sf}\}$, is defined by $\dot{\tilde{Q}}_f + C_f\ \tilde{Q}_f = C_f\ Q_f$. Furthermore, it follows that $\mathcal{V}_s \in L_\infty$ and $\mathcal{X}_{sf} \in L_\infty$.

Substituting (16) into (11) and using (18), (19), and (29) yield

$$\mathcal{A}_s \begin{bmatrix} \dot{\mathcal{V}}_{sf} \\ (1-\sigma_r)\ \dot{\mathcal{V}}_{sr} + \sigma_r\ \mathcal{F}_{sr} \end{bmatrix} = -\mathcal{A}_s^* \begin{bmatrix} \dot{\mathcal{V}}_{sf} \\ (1-\sigma_r)\ \dot{\mathcal{V}}_{sr} + \sigma_r\ \mathcal{F}_{sr} \end{bmatrix} + \mathcal{B}_s\ , \tag{32}$$

where

$$\begin{aligned}
\mathcal{A}_s &\triangleq (\mathcal{T}_s^T\ \mathcal{M}_s\ \mathcal{T}_s) \begin{bmatrix} I_{n_f} & 0 \\ 0 & (1-\sigma_r)\ I_{n_r} \end{bmatrix} + \begin{bmatrix} 0 & 0 \\ 0 & \sigma_r\ I_{n_r} \end{bmatrix}\ , \\
\mathcal{A}_s^* &\triangleq (\mathcal{T}_s^T\ \hat{\mathcal{M}}_s\ \mathcal{T}_s)\ A\ C \begin{bmatrix} \sigma_f\ M_f & 0 \\ 0 & \sigma_r\ I_{n_r} \end{bmatrix}\ , \\
\mathcal{B}_s &\triangleq (\mathcal{T}_s^T\ \hat{\mathcal{M}}_s\ \mathcal{T}_s) \left(\dot{\mathcal{V}}_{sd} + A\ C\ \tilde{\mathcal{F}}_s - \sigma_f\ A\ C \begin{bmatrix} D_f\ \dot{\tilde{\mathcal{X}}}_{sf} + \delta\ K_f\ \tilde{\mathcal{X}}_{sf} + (1-\delta)\ \varphi_f \\ 0 \end{bmatrix} \right)
\end{aligned}$$

$$+(\mathcal{T}_s^T\ \hat{\mathcal{M}}_s\ \dot{\mathcal{T}}_s + \mathcal{T}_s^T\ \hat{\mathcal{C}}_s\ \mathcal{T}_s)\ (\mathcal{V}_{sd} - A\ \tilde{\mathcal{F}}_s) + \mathcal{T}_s^T\ \hat{\mathcal{G}}_s + \begin{bmatrix} 0 \\ \sigma_r\ A_r^{-1}\ (C_r^{-1}\ \dot{\mathcal{V}}_{srd} + \mathcal{V}_{srd}) \end{bmatrix}$$
$$+\mathcal{K}_s\ \rho_s - (\mathcal{T}_s^T\ \mathcal{C}_s\ \mathcal{T}_s + \mathcal{T}_s^T\ \mathcal{M}_s\ \dot{\mathcal{T}}_s)\ \mathcal{V}_s - \mathcal{T}_s^T\ \mathcal{G}_s\ .$$

An algebraic loop about $\left[\dot{\mathcal{V}}_{sf}^T\ \ (1-\sigma_r)\ \dot{\mathcal{V}}_{sr}^T + \sigma_r\ \mathcal{F}_{sr}^T\right]^T$ is formed due to the first term in the right hand side of (32) which results from the control law (16) and (19). To preserve stability in a discrete implementation, a necessary and sufficient condition is that

$$\det\left(z\ I_6 + \mathcal{A}_s^{-1}\ \mathcal{A}_s^*\right) = 0 \tag{33}$$

has solutions inside the unit circle. In view of $\mathcal{A}_s^*$, this can be insured if there exists a positive constant σ_s such that

$$\|A\ C\| \leq \sigma_s\ . \tag{34}$$

Since $B_s \in L_\infty$, it follows that $\dot{\mathcal{V}}_s \in L_\infty$ and $\mathcal{F}_s \in L_\infty$. In view of (23), $\dot{\rho}_s \in L_\infty$ is achieved. Furthermore $\rho_s \to 0$ is obtained in terms of (29).

Theorem 2: For the slave robot incorporating a rigid/flexible environment (11) combined with the adaptive controller (16), (19), (18), (21), and the unilateral teleoperation controller (31), under the condition (34), it follows that

$$\begin{aligned} \mathcal{V}_{sfd} - \mathcal{V}_{sf} - A_f\ \tilde{\mathcal{F}}_{sf} &\longrightarrow 0\ , \quad \text{for constant } \sigma_f\ , \\ \mathcal{V}_{srd} - \mathcal{V}_{sr} &\longrightarrow 0\ , \quad \text{for } \sigma_r = 0\ , \\ \mathcal{V}_{srd} - A_r\ \tilde{\mathcal{F}}_{sr} &\longrightarrow 0\ , \quad \text{for } \sigma_r = 1\ . \end{aligned}$$

$\nabla\ \nabla\ \nabla$

This achieves impedance control for flexible environment contact, velocity tracking for approach motion, and force tracking for rigid environment contact within a frequency range $[0, \underline{\sigma}(C_r)/2\pi]$, where $\underline{\sigma}$ denotes the lowest singular value.

B. Bilateral Teleoperation

In bilateral motion/force teleoperation, the two design vectors $\mathcal{V}_{sd} \in R^6$ and $\mathcal{V}_{md} \in R^6$ are

specified as

$$\mathcal{V}_{sd} = \kappa_p \, (\tilde{\mathcal{V}}_m + \Lambda \, \tilde{\mathcal{P}}_m) - \delta \, \Lambda \, \mathcal{P}_s - A \, \kappa_f \, \tilde{\mathcal{F}}_m \, , \tag{35}$$

$$\mathcal{V}_{md} = \kappa_p^{-1} \, \left\{ \tilde{\mathcal{V}}_s + \delta \, \Lambda \, \tilde{\mathcal{P}}_s - \kappa_p \, \Lambda \, \mathcal{P}_m - A \, [\tilde{\mathcal{F}}_s + (\kappa_f - \kappa_p) \, \tilde{\mathcal{F}}_m] \right\} \, , \tag{36}$$

where $\kappa_p \in R^{6\times 6}$ and $\kappa_f \in R^{6\times 6}$ denote the motion scaling and force scaling matrices, respectively, from the master towards the slave, δ is a binary selective factor between the position-force control mode ($\delta = 1$) and the rate-force control mode ($\delta = 0$), $\Lambda \in R^{6\times 6} > 0$ is a diagonal control matrix, $\mathcal{P}_m$ and $\mathcal{P}_s$ denote the position/orientations of the master and the slave, respectively, subject to $\dot{\mathcal{P}}_m = \mathcal{V}_m$ and $\dot{\mathcal{P}}_s = \mathcal{V}_s$. Let $\tilde{Q}$, $Q = \{\mathcal{V}_m, \, \mathcal{V}_s, \, \mathcal{P}_m, \, \mathcal{P}_s\}$, be obtained by first order filtering

$$\dot{\tilde{Q}} + C \, \tilde{Q} = C \, Q \, . \tag{37}$$

The diagram of the complete bilateral teleoperation control system is illustrated in Fig. 2.

Remark 3.1: The teleoperation design (35) and (36) makes $\dot{\mathcal{V}}_{sd}$ and $\dot{\mathcal{V}}_{md}$ be functions of $\mathcal{V}_m$, $\mathcal{V}_s$, $\mathcal{F}_m$, and $\mathcal{F}_s$, in terms of (18) and (37). Therefore, no acceleration measurement is required by the controllers (16) and (17).

Remark 3.2: Note that $\mathcal{P}_s$ may involve Euler quaternions to express orientation. In order to avoid the unique singularity point corresponding to rotation of π, rate-force control should be employed for large rotations in free motion.

Substituting (35) and (36) into (29) and (30), and doing summation and subtraction yield

$$\rho_s - \kappa_p \, \rho_m = \kappa_p \, \tilde{\mathcal{V}}_m - \tilde{\mathcal{V}}_s + \Lambda \, [\kappa_p \, \tilde{\mathcal{P}}_m - \delta \, \tilde{\mathcal{P}}_s] + \kappa_p \, \mathcal{V}_m - \mathcal{V}_s + \Lambda \, [\kappa_p \, \mathcal{P}_m - \delta \, \mathcal{P}_s] \, , \tag{38}$$

$$\begin{aligned} \rho_s + \kappa_p \, \rho_m &= \kappa_p \, (\tilde{\mathcal{V}}_m - \mathcal{V}_m) + \tilde{\mathcal{V}}_s - \mathcal{V}_s \\ &\quad + \Lambda \, \kappa_p \, (\tilde{\mathcal{P}}_m - \mathcal{P}_m) + \delta \, \Lambda \, (\tilde{\mathcal{P}}_s - \mathcal{P}_s) - 2 \, A \, (\tilde{\mathcal{F}}_s + \kappa_f \, \tilde{\mathcal{F}}_m) \\ &= -C^{-1} \, \left(\kappa_p \, \dot{\tilde{\mathcal{V}}}_m + \dot{\tilde{\mathcal{V}}}_s + \Lambda \, \kappa_p \, \tilde{\mathcal{V}}_m + \delta \, \Lambda \, \tilde{\mathcal{V}}_s \right) \\ &\quad - 2 \, A \, (\tilde{\mathcal{F}}_s + \kappa_f \, \tilde{\mathcal{F}}_m) \, . \end{aligned} \tag{39}$$

Equation (38) can be rewritten as

$$\underline{\tilde{\mathcal{X}}} + \underline{\mathcal{X}} = \rho_s - \kappa_p \, \rho_m \, , \tag{40}$$

where

$$\underline{\mathcal{X}} \triangleq \kappa_p \, \mathcal{V}_m - \mathcal{V}_s + \Lambda \, [\kappa_p \, \mathcal{P}_m - \delta \, \mathcal{P}_s] \, , \tag{41}$$

$$\dot{\underline{\tilde{\mathcal{X}}}} + C \, \underline{\tilde{\mathcal{X}}} = C \, \underline{\mathcal{X}} \, . \tag{42}$$

Substituting (42) into (40) and using Lemma 1 yield $\dot{\underline{\tilde{\mathcal{X}}}} \in L_2 \bigcap L_\infty$, $\underline{\tilde{\mathcal{X}}} \in L_2 \bigcap L_\infty$, and further

$$\underline{\mathcal{X}} \in L_2 \bigcap L_\infty \, . \tag{43}$$

In case of position-force control ($\delta = 1$), it follows from (41), (43), and Lemma 1 that

$$\rho_p \triangleq \kappa_p \, \mathcal{V}_m - \mathcal{V}_s \in L_2 \bigcap L_\infty \, , \tag{44}$$

$$\rho_\epsilon \triangleq \kappa_p \, \mathcal{P}_m - \mathcal{P}_s \in L_2 \bigcap L_\infty \, . \tag{45}$$

This guarantees L_2 and L_∞ stability for both velocity and position errors, regardless of free motion or flexible/rigid contact motion.

In case of rate-force control ($\delta = 0$), it follows from (41) that

$$\rho_r \triangleq (\kappa_p \, \mathcal{V}_m + \Lambda \, \kappa_p \, \mathcal{P}_m) - \mathcal{V}_s \in L_2 \bigcap L_\infty \, . \tag{46}$$

This guarantees L_2 and L_∞ stability for an error between the slave velocity $\mathcal{V}_s$ and a combination of the master velocity and position denoted as $\kappa_p \, \mathcal{V}_m + \Lambda \, \kappa_p \, \mathcal{P}_m$.

In view of (44)-(46), equation (39) can be re-written as

$$-\frac{1}{2} \, \rho = A^{-1} \, C^{-1} \, (s + \Lambda) \, \kappa_p \, \tilde{\mathcal{V}}_m + (\tilde{\mathcal{F}}_s + \kappa_f \, \tilde{\mathcal{F}}_m) \, , \tag{47}$$

where

$$\rho \triangleq A^{-1} \, \left[-\delta \, C^{-1} \, (s + \Lambda) \, \tilde{\rho}_p - (1 - \delta) \, C^{-1} \, s \, \tilde{\rho}_r + (\rho_s + \kappa_p \, \rho_m) \right] \, ,$$

s denotes the Laplace operator, $\tilde{\rho}_p$ and $\tilde{\rho}_r$ are governed by $\dot{\tilde{\rho}}_p + C \, \tilde{\rho}_p = C \, \rho_p$ and $\dot{\tilde{\rho}}_r + C \, \tilde{\rho}_r = C \, \rho_r$ with ρ_p and ρ_r defined by (44) and (46). In view of Lemma 1, it follows that

$$\rho \in L_2 \bigcap L_\infty \, . \tag{48}$$

Four cases are studied as follows.

Case 1: When the slave is in free motion with $\sigma_f = 0$ and $\sigma_r = 0$, we have $\mathcal{F}_s = 0$. It follows from (12) and (47) that

$$\overline{\rho}_a = \overline{M}_a \ \dot{\tilde{\mathcal{V}}}_m + \overline{D}_a \ \tilde{\mathcal{V}}_m + \overline{D}_a \ \tilde{\mathcal{P}}_m \ , \tag{49}$$

where

$$\begin{aligned}
\overline{\rho}_a &\triangleq -\frac{1}{2} \ \rho - \kappa_f \ \tilde{\mathcal{F}}_h^* \ , \\
\overline{M}_a &\triangleq A^{-1} \ C^{-1} \ \kappa_p + \kappa_f \ M_h \ , \\
\overline{D}_a &\triangleq A^{-1} \ C^{-1} \ \Lambda \ \kappa_p + \kappa_f \ D_h \ , \\
\overline{K}_a &\triangleq \kappa_f \ K_h \ ,
\end{aligned}$$

and $\dot{\tilde{\mathcal{F}}}_h^* + C \ \tilde{\mathcal{F}}_h^* = C \ \mathcal{F}_h^*$. In term of Lemma 2, it follows from $\overline{\rho}_a \in L_\infty$ that $\tilde{\mathcal{P}}_m \in L_\infty$, $\tilde{\mathcal{V}}_m \in L_\infty$, and $\dot{\tilde{\mathcal{V}}}_m \in L_\infty$. Furthermore, it gives

$$\mathcal{V}_m \in L_\infty \ , \tag{50}$$

$$\mathcal{P}_m \in L_\infty \ , \tag{51}$$

$$\tilde{\mathcal{F}}_m \in L_\infty \ , \tag{52}$$

$$\mathcal{V}_s \in L_\infty \ . \tag{53}$$

Case 2: When the slave is in contact with the flexible environment with $\sigma_f = 1$ and $\sigma_r = 0$, it follows from (44) and (46) that

$$\mathcal{V}_s = \kappa_p \ \mathcal{V}_m - \delta \ \rho_p + (1 - \delta) \ (\Lambda \ \kappa_p \ \mathcal{P}_m - \rho_r) \ . \tag{54}$$

Furthermore, it follows from (47), (3), and (54) that

$$\overline{\rho}_b = \overline{M}_b \ \dot{\tilde{\mathcal{V}}}_m + \overline{D}_b \ \tilde{\mathcal{V}}_m + \overline{K}_b \ \tilde{\mathcal{P}}_m \ , \tag{55}$$

where

$$\begin{aligned}
\overline{\rho}_b \triangleq \ & \overline{\rho}_a + \mathrm{diag}\{M_f, 0\} \ [\delta \ \dot{\tilde{\rho}}_p + (1 - \delta) \ \dot{\tilde{\rho}}_r] + \mathrm{diag}\{D_f, 0\} \ [\delta \ \tilde{\rho}_p + (1 - \delta) \ \tilde{\rho}_r] \\
& + \delta \ \mathrm{diag}\{K_f, 0\} \ \rho_\epsilon - (1 - \delta) \ [\varphi_f^T, 0^T]^T \ ,
\end{aligned}$$

$$
\begin{aligned}
\overline{M}_b &\triangleq \overline{M}_a + \mathrm{diag}\{M_f, 0\}\ \kappa_p\ , \\
\overline{D}_b &\triangleq \overline{D}_a + (1-\delta)\ \mathrm{diag}\{M_f, 0\}\ \Lambda\ \kappa_p + \mathrm{diag}\{D_f, 0\}\ \kappa_p\ , \\
\overline{K}_b &\triangleq \overline{K}_a + (1-\delta)\ \mathrm{diag}\{D_f, 0\}\ \Lambda\ \kappa_p + \delta\ \mathrm{diag}\{K_f, 0\}\ \kappa_p\ .
\end{aligned}
$$

Note that $\overline{\rho}_b \in L_\infty$. It can be checked that equations (50)-(53) are still valid. Furthermore, it follows from (47) and (48) that

$$
\tilde{\mathcal{F}}_s \in L_\infty\ . \tag{56}
$$

Case 3: When the slave is in contact the rigid environment with $\sigma_f = 0$ and $\sigma_r = 1$, we have $\mathcal{V}_{sr} = [0, I_{n_r}]\ \mathcal{V}_s = 0$. In view of (44)-(46), it follows that $[0, I_{n_r}]\ \mathcal{V}_m \in L_\infty$ and $[0, I_{n_r}]\ \mathcal{P}_m \in L_\infty$. By following the steps of Case 1 and reducing dimension from 6 to n_f, $[I_{n_f}, 0]\ \mathcal{V}_m \in L_\infty$ and $[I_{n_f}, 0]\ \mathcal{P}_m \in L_\infty$ can be obtained. This yields $\tilde{\mathcal{F}}_m \in L_\infty$ from (12) and (14), and $\mathcal{V}_s \in L_\infty$ from (44)-(46). Furthermore, it follows from (47) that $\tilde{\mathcal{F}}_s \in L_\infty$. Thus, (50)-(53) and (56) hold.

Case 4: When the slave is in contact both the flexible and rigid environments with $\sigma_f = 1$ and $\sigma_r = 1$, results (50)-(53) and (56) are still valid by following the steps in Cases 2 and 3.

Lemma 3: Equations (50)-(53) and (56) hold for constant σ_f and σ_r.

$\nabla\ \nabla\ \nabla$

Substituting (16) into (11) and (17) into (15), and using (3), (12), (18), (19), (29), (30), (35), and (36) yield

$$
\begin{bmatrix} \mathcal{A}_m & 0 \\ 0 & \mathcal{A}_s \end{bmatrix}
\begin{bmatrix} \dot{\mathcal{V}}_m \\ \dot{\mathcal{V}}_{sf} \\ (1-\sigma_r)\ \dot{\mathcal{V}}_{sr} + \sigma_r\ \mathcal{F}_{sr} \end{bmatrix}
= -
\begin{bmatrix} \mathcal{A}^*_m & \mathcal{A}^*_{ms} \\ \mathcal{A}^*_{sm} & \mathcal{A}^*_s \end{bmatrix}
\begin{bmatrix} \dot{\mathcal{V}}_m \\ \dot{\mathcal{V}}_{sf} \\ (1-\sigma_r)\ \dot{\mathcal{V}}_{sr} + \sigma_r\ \mathcal{F}_{sr} \end{bmatrix}
+
\begin{bmatrix} \mathcal{B}^*_m \\ \mathcal{B}^*_s \end{bmatrix}\ , \tag{57}
$$

where $\mathcal{A}_s$ and $\mathcal{A}^*_s$ have been defined by (32), and

$$
\begin{aligned}
\mathcal{A}_m &\triangleq (\mathcal{T}_m^T\ \mathcal{M}_m\ \mathcal{T}_m) \in R^{6\times 6}\ , \\
\mathcal{A}^*_m &\triangleq (\mathcal{T}_m^T\ \hat{\mathcal{M}}_m\ \mathcal{T}_m)\ \kappa_f\ \kappa_p^{-1}\ A\ C\ M_h \in R^{6\times 6}\ , \\
\mathcal{A}^*_{ms} &\triangleq (\mathcal{T}_m^T\ \hat{\mathcal{M}}_m\ \mathcal{T}_m)\ \kappa_p^{-1}\ A\ C \begin{bmatrix} \sigma_f\ M_f & 0 \\ 0 & \sigma_r\ I_{n_r} \end{bmatrix} \in R^{6\times 6}\ , \\
\mathcal{A}^*_{sm} &\triangleq \left[(\mathcal{T}_s^T\ \hat{\mathcal{M}}_s\ \mathcal{T}_s)\ A\ C + \sigma_r\ \mathrm{diag}\{0, I_{n_r}\}\right]\ \kappa_f\ M_h \in R^{6\times 6}\ ,
\end{aligned}
$$

$$
\begin{aligned}
\mathcal{B}_m^* \;\triangleq\; & -\mathcal{T}_m^T\ \hat{\mathcal{M}}_m\ \mathcal{T}_m\ \left\{\kappa_p^{-1}\ A\ C\ \left[\begin{array}{c}\sigma_f\ [D_f\ \dot{\mathcal{X}}_{sf}+\delta\ K_f\ \mathcal{X}_{sf}+(1-\delta)\ \varphi_f]\\ 0\end{array}\right]\right. \\
& +\kappa_p^{-1}\ \kappa_f\ A\ C\ (D_h\ \dot{\mathcal{X}}_h+K_h\ \mathcal{X}_h+\mathcal{F}_h^*) \\
& \left.-\kappa_p^{-1}\ \left[\dot{\tilde{\mathcal{V}}}_s+\delta\ \Lambda\ \tilde{\mathcal{V}}_s-\kappa_p\ \Lambda\ \mathcal{V}_m+A\ C\ (\tilde{\mathcal{F}}_s+\kappa_f\ \tilde{\mathcal{F}}_m)\right]\right\} \\
& +(\mathcal{T}_m^T\ \hat{\mathcal{M}}_m\ \dot{\mathcal{T}}_m+\mathcal{T}_m^T\ \hat{\mathcal{C}}_m\ \mathcal{T}_m)\ (\rho_m+\mathcal{V}_m)+\mathcal{T}_m^T\ \hat{\mathcal{G}}_m+\mathcal{K}_m\ \rho_m \\
& +\alpha_h\ \mathrm{sign}(\rho_m)-(\mathcal{T}_m^T\ \mathcal{C}_m\ \mathcal{T}_m+\mathcal{T}_m^T\ \mathcal{M}_m\ \dot{\mathcal{T}}_m)\ \mathcal{V}_m-\mathcal{T}_m^T\ \mathcal{G}_m-\mathcal{F}_h^*\in R^6\ , \\
\mathcal{B}_s^* \;\triangleq\; & -\mathcal{T}_s^T\ \hat{\mathcal{M}}_s\ \mathcal{T}_s\ A\ C\ \left[\begin{array}{c}\sigma_f\ [D_f\ \dot{\mathcal{X}}_{sf}+\delta\ K_f\ \mathcal{X}_{sf}+(1-\delta)\ \varphi_f]\\ 0\end{array}\right] \\
& -\left(\mathcal{T}_s^T\ \hat{\mathcal{M}}_s\ \mathcal{T}_s\ A\ C+\mathrm{diag}\{0,\sigma_r\ I_{n_r}\}\right)\ \kappa_f\ (D_h\ \dot{\mathcal{X}}_h+K_h\ \mathcal{X}_h+\mathcal{F}_h^*) \\
& +\mathcal{T}_s^T\ \hat{\mathcal{M}}_s\ \mathcal{T}_s\ \left[\kappa_p\ (\dot{\tilde{\mathcal{V}}}_m+\Lambda\ \tilde{\mathcal{V}}_m)-\delta\ \Lambda\ \mathcal{V}_s+A\ C\ (\tilde{\mathcal{F}}_s+\kappa_f\ \tilde{\mathcal{F}}_m)\right] \\
& +(\mathcal{T}_s^T\ \hat{\mathcal{M}}_s\ \dot{\mathcal{T}}_s\ +\mathcal{T}_s^T\ \hat{\mathcal{C}}_s\ \mathcal{T}_s)\ (\rho_s+\mathcal{V}_s)+\mathcal{T}_s^T\ \hat{\mathcal{G}}_s \\
& +\mathrm{diag}\{0,\sigma_r\ I_{n_r}\}\ [A^{-1}\ \kappa_p\ (\mathcal{V}_m+\Lambda\ \mathcal{P}_m)-\delta\ A^{-1}\ \Lambda\ (C^{-1}\ \mathcal{V}_s+\mathcal{P}_s)]+\mathcal{K}_s\ \rho_s \\
& -(\mathcal{T}_s^T\ \mathcal{C}_s\ \mathcal{T}_s+\mathcal{T}_s^T\ \mathcal{M}_s\ \dot{\mathcal{T}}_s)\ \mathcal{V}_s-\mathcal{T}_s^T\ \mathcal{G}_s\in R^6\ .
\end{aligned}
$$

In view of Lemma 3 and Lemma 1, $\mathcal{B}_m^* \in L_\infty$ and $\mathcal{B}_s^* \in L_\infty$ can be ensured. Note that $\mathcal{A}_m^*$, $\mathcal{A}_{ms}^*$, and $\mathcal{A}_s^*$ are continuous about $A\ C$, and are zero when $A\ C = 0$. Therefore, there exists a positive constant σ_b such that for

$$\|A\ C\| \leq \sigma_b\ , \tag{58}$$

the solutions of

$$\det\left(z\ I_{12}+\left[\begin{array}{cc}\mathcal{A}_m^{-1}\ \mathcal{A}_m^* & \mathcal{A}_m^{-1}\ \mathcal{A}_{ms}^*\\ \mathcal{A}_s^{-1}\ \mathcal{A}_{sm}^* & \mathcal{A}_s^{-1}\ \mathcal{A}_s^*\end{array}\right]\right)=0 \tag{59}$$

are within the unit circle. Thus, it follows that $\dot{\mathcal{V}}_m \in L_\infty$, $\dot{\mathcal{V}}_s \in L_\infty$, $\mathcal{F}_m \in L_\infty$, and $\mathcal{F}_s \in L_\infty$. Finally, it follows from (23) and (24) that $\dot{\rho}_s \in L_\infty$ and $\dot{\rho}_m \in L_\infty$. This indicates that ρ_s and ρ_m defined by (29) and (30) are uniformly continuous functions in L_2 and L_∞. This implies

$$\rho_s \;\longrightarrow\; 0\ , \tag{60}$$

$$\rho_m \;\longrightarrow\; 0 \tag{61}$$

for constant σ_f and σ_r. Consequently, it follows that

$$\kappa_p\ \mathcal{V}_m-\mathcal{V}_s \;\longrightarrow\; 0 \tag{62}$$

$$\kappa_p \ \mathcal{P}_m - \mathcal{P}_s \quad \longrightarrow \quad 0 \tag{63}$$

in position-force control and

$$(\kappa_p \ \mathcal{V}_m + \Lambda \ \kappa_p \ \mathcal{P}_m) - \mathcal{V}_s \longrightarrow 0 \tag{64}$$

in rate-force control.

To study the transparency of the complete teleoperation system, (47) can be re-written as

$$-\tilde{\mathcal{F}}_m = \kappa_f^{-1} \ \tilde{\mathcal{F}}_s + \kappa_f^{-1} \ \kappa_p \ A^{-1} \ C^{-1} \ (s + \Lambda) \ \tilde{\mathcal{V}}_m + \frac{1}{2} \ \kappa_f^{-1} \ \rho \ . \tag{65}$$

Remark 3.3: This equation summarizes the transparency properties of the complete teleoperation system. Within a certain frequency range bounded by $\underline{\sigma}(C)/2\pi$, we have $\tilde{\mathcal{F}}_m \approx \mathcal{F}_m$, $\tilde{\mathcal{F}}_s \approx \mathcal{F}_s$, and $\tilde{\mathcal{V}}_m \approx \mathcal{V}_m$. Note that $\rho \to 0$. The term in the left hand side denotes the force from the operator toward the master. The first term in the right hand side devotes the contribution of the operator force to the task execution. The second term indicates that the teleoperation system behaves as a free-floating mass $\kappa_f^{-1} \ \kappa_p \ A^{-1} \ C^{-1}$ plus a linear damper $\kappa_f^{-1} \ \kappa_p \ A^{-1} \ C^{-1} \ \Lambda$, which are completely specified by control and scaling parameters instead of system parameters. In fact, the equivalent mass and damper contribute to transparency error. In order to reduce the transparency error, large A and C are required. However, they are limited by (58) for maintaining the stability of an algebraic loop specified by (57). Therefore, the choice of A and C specifies the trade-off between stability and transparency. Another way to reduce transparency errors is to use small motion scaling κ_p and large force scaling κ_f, subject to task specification.

The results of bilateral teleoperation control in both position-force control mode and rate-force control mode can be summarized into the following theorem:

Theorem 3: For a bilateral teleoperated system in which both the master and the slave are subject to independent adaptive motion/force control and satisfy (29) and (30), applying the teleoperation controller design (35) and (36) results in:

a) L_2 and L_∞ stability for both free motion and flexible/rigid contact motion in the sense of (44) and (45) with position-force control and (46) with rate-force control;

b) asymptotic motion (velocity/position) tracking for both free motion and flexible/rigid contact motion in the sense of (62) and (63) with position-force control and (64) with rate-force control; and

c) within a certain frequency range bounded by $\underline{\sigma}(C)/2\pi$, the overall teleoperation system is equivalent to a free-floating mass $\kappa_f^{-1}\ \kappa_p\ A^{-1}\ C^{-1}$ plus a linear damper $\kappa_f^{-1}\ \kappa_p\ A^{-1}\ C^{-1}\ \Lambda$, specified by control and scaling parameters.

$\nabla\ \nabla\ \nabla$

Remark 3.4: In case of no parameter uncertainty, it is obvious that exponential stability and convergence can be achieved in terms of (25)-(28).

C. The Issue of Time Delay

When time delays appear in the communication channels between the master and the slave, (35) and (36) have to be modified to

$$\mathcal{V}_{sd} = e^{-sT}\ \kappa_p\ (\tilde{\mathcal{V}}_m + \Lambda\ \tilde{\mathcal{P}}_m) - \delta\ \Lambda\ \mathcal{P}_s - e^{-sT}\ A\ \kappa_f\ \tilde{\mathcal{F}}_m\ , \tag{66}$$

$$\mathcal{V}_{md} = \kappa_p^{-1}\ \left\{e^{-sT}\ (\tilde{\mathcal{V}}_s + \delta\ \Lambda\ \tilde{\mathcal{P}}_s) - \kappa_p\ \Lambda\ \mathcal{P}_m - A\ [e^{-sT}\ \tilde{\mathcal{F}}_s + (\kappa_f - \kappa_p)\ \tilde{\mathcal{F}}_m]\right\}\ . \tag{67}$$

Substituting (66) and (67) into (29) and (30) yields

$$\mathcal{V}_s + \delta\ \Lambda\ \mathcal{P}_s + A\ \tilde{\mathcal{F}}_s = e^{-sT}\ [\kappa_p\ (\tilde{\mathcal{V}}_m + \Lambda\ \tilde{\mathcal{P}}_m) - A\ \kappa_f\ \tilde{\mathcal{F}}_m] - \rho_s\ , \tag{68}$$

$$\kappa_p\ (\mathcal{V}_m + \Lambda\ \mathcal{P}_m) + A\ \kappa_f\ \tilde{\mathcal{F}}_m = e^{-sT}\ (\tilde{\mathcal{V}}_s + \delta\ \Lambda\ \tilde{\mathcal{P}}_s - A\ \tilde{\mathcal{F}}_s) - \kappa_p\ \rho_m\ , \tag{69}$$

where T is the one way delay. Assume that

$$\mathcal{F}_s = \mathcal{Z}_e\ \mathcal{V}_s \tag{70}$$

$$\mathcal{F}_m = \mathcal{Z}_h\ \mathcal{V}_m + \mathcal{F}_h^*\ , \tag{71}$$

i.e. no rigid contact is considered. It follows from (68) and (69) that

$$\mathcal{G}_{1s}(s)\ (\tilde{\mathcal{P}}_s) = \mathcal{G}_{2s}(s)\ e^{-sT}\ (\kappa_p \tilde{\mathcal{P}}_m) - \underline{\rho}_s\ , \tag{72}$$

$$\mathcal{G}_{1m}(s)\ (\kappa_p \tilde{\mathcal{P}}_m) = \mathcal{G}_{2m}(s)\ e^{-sT}\ (\tilde{\mathcal{P}}_s) - \kappa_p\ \underline{\rho}_m\ , \tag{73}$$

where

$$\underline{\rho}_s \triangleq \rho_s + e^{-sT}\ A\ \kappa_f\ \tilde{\mathcal{F}}_h^* \ , \tag{74}$$

$$\underline{\rho}_m \triangleq \rho_m + A\ \kappa_f\ \kappa_p^{-1}\ \tilde{\mathcal{F}}_h^* \ , \tag{75}$$

$$\mathcal{G}_{1s}(s) \triangleq (s+\delta\ \Lambda)\ (C^{-1}\ s + I_6) + A\ \mathcal{Z}_e\ s \ , \tag{76}$$

$$\mathcal{G}_{2s}(s) \triangleq (s+\Lambda)\ I_6 - A\ \kappa_f\ \kappa_p^{-1}\ \mathcal{Z}_h\ s \ , \tag{77}$$

$$\mathcal{G}_{1m}(s) \triangleq (s+\Lambda)\ (C^{-1}\ s + I_6) + A\ \kappa_f\ \kappa_p^{-1}\ \mathcal{Z}_h\ s \ , \tag{78}$$

$$\mathcal{G}_{2m}(s) \triangleq (s+\delta\ \Lambda)\ I_6 - A\ \mathcal{Z}_e\ s \ . \tag{79}$$

Combining (72) and (73) yields

$$\tilde{\mathcal{P}}_s = \mathcal{G}_{1s}(s)^{-1}\ \mathcal{G}_{2s}(s)\ \mathcal{G}_{1m}(s)^{-1}\ \mathcal{G}_{2m}(s)\ e^{-2sT}\ \tilde{\mathcal{P}}_s - \rho_s^* \ , \tag{80}$$

$$\kappa_p\ \tilde{\mathcal{P}}_m = \mathcal{G}_{1m}(s)^{-1}\ \mathcal{G}_{2m}(s)\ \mathcal{G}_{1s}(s)^{-1}\ \mathcal{G}_{2s}(s)\ e^{-2sT}\ (\kappa_p\ \tilde{\mathcal{P}}_m) - \rho_m^* \ , \tag{81}$$

where

$$\rho_s^* = \mathcal{G}_{1s}(s)^{-1}\ \underline{\rho}_s + \mathcal{G}_{1s}(s)^{-1}\ \mathcal{G}_{2s}(s)\ \mathcal{G}_{1m}(s)^{-1}\ e^{-sT}\ \kappa_p\ \underline{\rho}_m \ ,$$

$$\rho_m^* = \mathcal{G}_{1m}(s)^{-1}\ \kappa_p\ \underline{\rho}_m + \mathcal{G}_{1m}(s)^{-1}\ \mathcal{G}_{2m}(s)\ \mathcal{G}_{1s}(s)^{-1}\ e^{-sT}\ \underline{\rho}_s \ .$$

The sufficient condition to ensure stability for any time delay is

$$\begin{cases} \|\mathcal{G}_{1s}(j\omega)^{-1}\ \mathcal{G}_{2s}(j\omega)\ \mathcal{G}_{1m}(j\omega)^{-1}\ \mathcal{G}_{2m}(j\omega)\|_\infty < 1 \\ \|\mathcal{G}_{1m}(j\omega)^{-1}\ \mathcal{G}_{2m}(j\omega)\ \mathcal{G}_{1s}(j\omega)^{-1}\ \mathcal{G}_{2s}(j\omega)\|_\infty < 1 \ . \end{cases} \tag{82}$$

Two examples are given below.

The first example is free motion of both the master and the slave, i.e. $\mathcal{F}_h^* = \mathcal{F}_m = \mathcal{F}_s = 0$. Therefore, $\mathcal{Z}_h = \mathcal{Z}_e = 0$. It follows from (76)-(79) and (82) that

$$\begin{aligned} \|\mathcal{G}_{1s}(j\omega)^{-1}\ \mathcal{G}_{2s}(j\omega)\ \mathcal{G}_{1m}(j\omega)^{-1}\ \mathcal{G}_{2m}(j\omega)\|_\infty &= \|\mathcal{G}_{1m}(j\omega)^{-1}\ \mathcal{G}_{2m}(j\omega)\ \mathcal{G}_{1s}(j\omega)^{-1}\ \mathcal{G}_{2s}(j\omega)\|_\infty \\ &= \|(j\omega\ I_6 + C)^{-1}\ C\ (j\omega\ I_6 + C)^{-1}\ C\|_\infty \\ &< 1 \ , \end{aligned} \tag{83}$$

since C is a positive-definite diagonal matrix.

The second example is a one-dimensional case with

$$\mathcal{Z}_h = m_h\ s + b_h + \frac{k_h}{s}\ , \tag{84}$$

$$\mathcal{Z}_e = m_e\ s + b_e + \frac{k_e}{s}\ . \tag{85}$$

It follows that

$$\begin{aligned} \|\mathcal{G}_{1s}(j\omega)^{-1}\ \mathcal{G}_{2s}(j\omega)\ \mathcal{G}_{1m}(j\omega)^{-1}\ \mathcal{G}_{2m}(j\omega)\|_\infty &= \|\mathcal{G}_{1m}(j\omega)^{-1}\ \mathcal{G}_{2m}(j\omega)\ \mathcal{G}_{1s}(j\omega)^{-1}\ \mathcal{G}_{2s}(j\omega)\|_\infty \\ &= \max_\omega \left| \frac{(j\omega + \delta\ \Lambda) - A\ j\omega\ \mathcal{Z}_e}{(j\omega + \delta\ \Lambda)(\frac{j\omega}{C} + 1) + A\ j\omega\ \mathcal{Z}_e} \right. \\ &\qquad \left. \frac{(j\omega + \Lambda) - \frac{\kappa_f}{\kappa_p}\ A\ j\omega\ \mathcal{Z}_h}{(j\omega + \Lambda)(\frac{j\omega}{C} + 1) + \frac{\kappa_f}{\kappa_p}\ A\ j\omega\ \mathcal{Z}_h} \right| . \end{aligned} \tag{86}$$

The sufficient conditions to ensure (82) are given by

$$\begin{aligned} k_e &< 2\ C\ b_e\ , \\ m_e &< \frac{1}{2\ C}\ b_e + \frac{\Lambda}{4\ A\ C^2}\ , \\ k_h &< 2\ C\ b_h\ , \\ m_h &< \frac{1}{2\ C}\ b_h + \frac{\Lambda\ \kappa_p}{4\ \kappa_f\ A\ C^2} + \frac{k_h}{C\ \Lambda} + \sqrt{\left(\frac{k_h}{C\Lambda}\right)^2 + \frac{k_h}{AC^2\Lambda}\frac{\kappa_p}{\kappa_f}} \end{aligned}$$

These conditions can be satisfied by appropriately choosing control parameters providing that the damping coefficients b_e and b_h are positive. A large C satisfies the constraints for k_e and k_h, while a small A satisfies the constraints for m_e and m_h.

IV Experiments

A. System Set-up

A photograph of the experimental set-up is shown in Fig. 3. It consists of a one-axis master and a one-axis slave driven by MAXON Motors RE 035-071 with 4,000 pulse encoders. A planetary gearhead with 10:1 ratio and a harmonic drive with 50:1 ratio are mounted at the master site and at the slave site, respectively, to increase torques. Two force sensors UFS 3012A25 U560 by JR^3 Inc. are used at the end-effectors of both the master and the slave. The distances between the centers

of the force sensors to the motor driving axes are 65mm for the master and 132mm for the slave, respectively. A handle for the operator is mounted on the force sensor of the master. An aluminum bar with a 25mm diameter is mounted to the base for *rigid* contact experiments with the slave. When soft tissues, e.g. a person's hand, are put between the aluminum bar and the slave, a $flexible$ contact is realized. The friction forces reflected at the end-effectors of the master and slave robots are of the order of $0.4N$ and $6.0N$, respectively. The feedback gains in (16) and (17) are set as $\mathcal{K}_m = 80.0$ and $\mathcal{K}_s = 800.0$. The estimates of d_j in (8) result in strong integrals of (29) and (30), see (21). The integral gains are set as $\rho^m_{d_j} = 2,400.0N/m$ and $\rho^s_{d_j} = 20,000.0N/m$. The control system is running with two sampling frequencies on a SPARC 1E VME board by FORCE COMPUTERS Inc. using the VxWorks operating system. The high sampling frequency of 500Hz is used to calculate (16), (17), (35), and (36), while the low sampling frequency of 100Hz is used to calculate (18), (21), and (37). The sampling frequency for feedback control must be high to achieve good dynamic performance, while the sampling frequency for filter calculations may be lower. The experimental results are illustrated from Fig. 4 to Fig. 10. In these figures, solid lines represent the scaled motion/forces of the master and dashed lines represent the exact motion/forces of the slave.

B. Position-Force Teleoperation with Rigid/Flexible Contact

Fig. 4 illustrates experimental results for position-force teleoperation with $\kappa_p = 1.0$ and $\kappa_f = 10.0$. Control parameters are set to $A = 0.0005$, $C = 50.0$, and $\Lambda = 1.0$, which yield an equivalent mass of $4kg$ and an equivalent damping of $4Ns/m$ in terms of (65). The control parameter C is chosen such that $C/2\pi \approx 8Hz$ represents the interested control frequency range. The motion scaling κ_p is chosen in terms of the task requirement. After κ_p and C are specified, the force scaling κ_f and the force control gain A should be chosen as large as possible to reduce the equivalent mass and damping, while maintaining reasonably good kinesthetic feedback, and subject to (58). The system starts in free motion and then contacts the rigid aluminum bar around $t = 5.5s$. Fig 4a) shows excellent position tracking in both free motion and rigid contact. Fig 4b) shows very good force tracking during contact. The rigid contact is very smooth. There is no bouncing during contact. The large force error in free

motion results from the fact that the teleoperation system behaves as a mass of $4kg$ plus a damping of $4Ns/m$. Note that the force of the master (solid line) is scaled by a factor of 10.

Fig. 5 illustrates experimental results for position-force teleoperation in flexible contact. A human palm is put between the slave and the aluminum bar. The contact occurs just after $t = 6s$. Scaling parameters are $\kappa_p = 1.0$ and $\kappa_f = 2.0$. Control parameters are $A = 0.002$, $C = 50.0$, and $\Lambda = 1.0$. The tracking results for both position and force are quite comparable with Fig. 4.

Fig. 6 and Fig. 7 illustrate position-force teleoperation results in rigid contact with different scaling parameters. Fig. 6 is with $\kappa_p = 0.5$ and $\kappa_f = 5.0$; while Fig. 7 is with $\kappa_p = 2.0$ and $\kappa_f = 20.0$. Control parameters are the same as Fig. 4. The large force noise in Fig. 7b) results from high force scaling. These results are quite comparable to Fig. 4.

C. Rate-Force Teleoperation with Rigid/Flexible Contact

Fig. 8 and Fig. 9 illustrate experimental results in rate-force teleoperation with rigid and flexible constraints. Fig. 8 gives results in rigid contact. Scaling parameters are $\kappa_p = 1.0$, $\Lambda = 10.0$ and $\kappa_f = 10.0$. Control parameters are $A = 0.0005$ and $C = 50.0$. Fig. 8a) shows the velocity tracking error, while Fig. 8b) shows the force tracking error. Excellent velocity tracking is achieved in both free motion and rigid contact occurred after $t = 5.0s$. Force tracking is still very good. There is no bouncing during transition phases from free motion to rigid contact. The solid line in Fig. 8(a) denotes a combination of velocity and position of the master, i.e. $\mathcal{V}_m + \Lambda\mathcal{P}_m$. Therefore, the position of the master goes to zero after rigid contact, while a non-zero contact force is applied.

Fig. 9 shows experimental results in flexible contact. Scaling parameters are $\kappa_p = 1.0$, $\Lambda = 10.0$, $\kappa_f = 2.0$ and control parameters are $A = 0.002$, $C = 50.0$. A human palm is put between the rigid aluminum bar and the slave. The tracking performance for both velocity and force is quite comparable to Fig. 8.

Remark 4.1: The experimental results match the theoretical results very well despite of using very simple second order LTI models for both the flexible environment and the human operator. Although the issue of transitions between free and contact motion has not been addressed theoretically, the

experimental results demonstrate very smooth and passive behavior at these transitions. The following two experiments demonstrate this point. In the first experiment, the slave is controlled (by the master) to touch the rigid bar. Then the master handle is released by the operator. The slave is still in contact with the rigid bar with almost zero contact force. In the second experiment, the master handle is released. The teleoperation system behaves exactly as a free-floating mass plus a damper. When a pulse force is applied to the handle, the teleoperation master and slave move in the same direction as the pulse force. After contact with the rigid bar, the teleoperation system is reflected back, but it does not reach the original position because of damping.

D. Time Delay

A fixed time delay was implemented for both motion and force transmission from the master site to the slave site and *vice versa*. Experiments reveal that stability is maintained for any time delay in both free motion and contact motion. The motion/force tracking ability is maintained until the one-way time delay reaches approximately 0.1 (100ms) seconds. For larger dealys, the tracking ability decreases quickly. The teleoperation system behaves as a wave-reflector with less damping when the one-way time delay reaches 0.2 seconds. For one-way time delays of over 10 seconds, the system behaves as two independent motion/force controlled subsystems. Fig. 10 illustrates the experimental results of position-force teleoperation when the one-way time delay is 0.1 seconds. The results are still comparable with Fig. 4.

V Discussion

Lawrence [14] suggested to use a four-channel communication structure for transparent teleoperation controller design. It is worthwhile to view this proposed scheme from the point of view of Lawrence's structure.

In view of (35)-(36) and Fig. B1(b), the block diagram of an 1-DOF teleoperation system is illustrated in Fig. 11, where

$$C_m \;=\; K_m + \frac{K_{mI}}{s} - (\hat{b}_h + \frac{\hat{k}_h}{s}) \,, \tag{87}$$

$$G_m^b = (\hat{M}_m + \hat{m}_h)\ s + K_m + \frac{K_{mI}}{s}\ , \tag{88}$$

$$G_m^a = \frac{AC}{s+C}\ G_m^b\ , \tag{89}$$

$$C_s = K_s + \frac{K_{sI}}{s} - (\hat{b}_e + \frac{\hat{k}_e}{s})\ , \tag{90}$$

$$G_s^b = (\hat{M}_s + \hat{m}_e)\ s + K_s + \frac{K_{sI}}{s}\ , \tag{91}$$

$$G_s^a = \frac{AC}{s+C}\ G_s^b\ , \tag{92}$$

$$C_1 = \frac{(s+\Lambda)C}{s(s+C)}\ \kappa_p\ G_s^b\ , \tag{93}$$

$$C_2 = \frac{1}{\kappa_p}\ G_m^a\ , \tag{94}$$

$$C_3 = \kappa_f\ G_s^a\ , \tag{95}$$

$$C_4 = \frac{(s+\delta\Lambda)C}{s(s+C)}\ \frac{1}{\kappa_p}\ G_m^b\ . \tag{96}$$

The constant disturbance d_x in Fig. A1(b) is not included, since it can be completely compensated by integral control. By defining

$$G_m^* \triangleq M_m\ s + C_m + \frac{\Lambda}{s}\ G_m^b\ , \tag{97}$$

$$G_s^* \triangleq M_s\ s + C_s + \frac{\delta\Lambda}{s}\ G_s^b\ , \tag{98}$$

it follows from Fig. 11 that

$$G_m^*\ \mathcal{V}_m + \left(1 + \frac{\kappa_f}{\kappa_p}\ G_m^a\right)\ \mathcal{F}_m = \frac{1}{\kappa_p}\ \frac{(s+\delta\Lambda)C}{s(s+C)}\ G_m^b\ \mathcal{V}_s - \frac{1}{\kappa_p}\ \frac{AC}{s+C}\ G_m^b\ \mathcal{F}_s\ , \tag{99}$$

$$G_s^*\ \mathcal{V}_s + (1 + G_s^a)\ \mathcal{F}_s = \kappa_p\ \frac{(s+\Lambda)C}{s(s+C)}\ G_s^b\ \mathcal{V}_m - \kappa_f\ \frac{AC}{s+C}\ G_s^b\ \mathcal{F}_m\ . \tag{100}$$

Note that

$$s\ (G_m^* + \mathcal{Z}_h) = (s+\Lambda)\ G_m^b + \xi_h\ , \tag{101}$$

$$s\ (G_s^* + \mathcal{Z}_e) = (s+\delta\Lambda)\ G_s^b + \xi_e\ , \tag{102}$$

where $\mathcal{Z}_h$ and $\mathcal{Z}_e$ are defined in (84) and (85), while

$$\xi_h \triangleq (M_m + m_h - \hat{M}_m - \hat{m}_h)\ s^2 + (b_h - \hat{b}_h)\ s + (k_h - \hat{k}_h)\ ,$$

$$\xi_e \triangleq (M_s + m_e - \hat{M}_s - \hat{m}_e)\ s^2 + (b_e - \hat{b}_e)\ s + (k_e - \hat{k}_e)\ .$$

Assume $\mathcal{F}_h^* = 0$, i.e. that the exogenous force is completely compensated by α_h sign(ρ_m). Applying (101) and (102) into (99) and (100), and using $\mathcal{F}_m = \mathcal{Z}_h\ \mathcal{V}_m$ and $\mathcal{F}_s = \mathcal{Z}_e\ \mathcal{V}_s$ lead to

$$\left(\kappa_p\ \frac{s+\Lambda}{s} + \kappa_f\ \frac{AC}{s+C}\ \mathcal{Z}_h\right)\ \mathcal{V}_m \;=\; \left(\frac{(s+\delta\Lambda)C}{s(s+C)} - \frac{AC}{s+C}\ \mathcal{Z}_e\right)\ \mathcal{V}_s - \frac{\kappa_p}{s}\ \xi_h\ , \tag{103}$$

$$\left(\frac{s+\delta\Lambda}{s} + \frac{AC}{s+C}\ \mathcal{Z}_e\right)\ \mathcal{V}_s \;=\; \left(\kappa_p\ \frac{(s+\Lambda)C}{s(s+C)} - \kappa_f\ \frac{AC}{s+C}\ \mathcal{Z}_h\right)\ \mathcal{V}_m - \frac{1}{s}\ \xi_e\ . \tag{104}$$

Changing the sides of (104) and summing with (103) yields

$$(s+2\ C)(s+\Lambda)\ \kappa_p \mathcal{V}_m = (s+2\ C)(s+\delta\ \Lambda)\ \mathcal{V}_s + (s+C)(\xi_e - \kappa_p\ \xi_h)\ . \tag{105}$$

When the effects of ξ_h and ξ_e are compensated by parameter adaptation, i.e. $\xi_h = \xi_e = 0$, it follows that

$$(s+\delta\ \Lambda)\ \mathcal{V}_s = (s+\Lambda)\ \kappa_p \mathcal{V}_m\ . \tag{106}$$

This equation is consistent with (44)-(46) and (62)-(64).

Meanwhile, when $\xi_h = \xi_e = 0$ (i.e. the effects of parameter uncertainty are compensated by parameter adaptation), multiplying (103) by (104) results in

$$-\mathcal{Z}_h = \frac{\kappa_p}{\kappa_f}\ \frac{s+\Lambda}{s+\delta\ \Lambda}\ \mathcal{Z}_e + \frac{\kappa_p}{\kappa_f}\ \frac{s+\Lambda}{A\ C}\ . \tag{107}$$

This equation is consistent with (65). $-\mathcal{Z}_h = -\mathcal{F}_m/\mathcal{V}_m$ denotes the impedance of the teleoperation system viewed from the operator site. The first term on the right hand side represents the environment impedance reflected to the operator site. When in position-force control, where $\delta = 1$, the first term in the right hand side becomes $(\kappa_p/\kappa_f)\ \mathcal{Z}_e$, i.e. the impedance of the environment reflected to the master through motion and force scaling. When in velocity-force control, where $\delta = 0$, it becomes $\frac{\kappa_p}{\kappa_f}\ \frac{s+\Lambda}{s}\ \mathcal{Z}_e$, which reflects scaled environment impedance $(\kappa_p/\kappa_f)\ \mathcal{Z}_e$ only at high frequency, where $(s+\Lambda)/s \to 1$. The second term on the right hand side indicates that the teleoperation system behaves as a mass $\frac{\kappa_p}{\kappa_f}\ \frac{1}{A\ C}$ plus a damper $\frac{\kappa_p}{\kappa_f}\ \frac{\Lambda}{A\ C}$. Note that the transparency error is completely characterized by this term, which is independent of the control modes used.

Remark 5.1: The structure of the proposed approach, see Fig. 11, is similar to Lawrence's structure [14]. They all have four communication channels. However, as can be explained in Fig.

1, the principle used in designing these channels is different. The communication channels C_1 to C_4 in Lawrence's approach perform inverse dynamic control. C_1 to C_4 are designed to cancel the dynamics of both master and slave robots so as to achieve a perfectly transparent block. However, inverse dynamic control is very sensitive to uncertainties. Therefore, a small time delay and any dynamic uncertainty, such as joint friction, may considerably deteriorate system performance and may further cause instability. In the proposed approach, the master together with the operator, and the slave together with the environment, are treated as two separate blocks. Each block is subject to independent adaptive motion/force control. Therefore, the uncertainties in each block are well compensated by strong feedback control together with parameter adaptation. Compared to Fig. 2 in [14], there are two additional local force feedback loops in Fig. 11 formed by $\frac{\kappa_f}{\kappa_p}\, G_m^a$ and G_s^a, respectively, to enhance force control ability. The communication channels only transform the motion/force information from the master toward the slave and from the slave toward the master. Therefore, the method proposed here is robust against uncertainties including time delay. Within a pre-specified frequency range, the teleoperation system is equivalent to a linearly-damped free-floating mass, specified by control and scale parameters only. This feature produces excellent motion (position/velocity) tracking and very good force tracking. The force tracking accuracy can be improved further by using a large force scaling κ_f. The motion/force tracking is a new and important feature of the proposed controller, which is not achieved by previous stability-guaranteed designs [10], [12], and [13].

Remark 5.2: In contrast to transparency-based rate control [27, 28], the adaptive motion/force control presented here does not return the derivative of the environment force to the master. Although transparency is lost, the method does not have the drawback of transforming unilateral contraints into bilateral ones ("sticking" behaviour) [27, 28]).

Remark 5.3: The teleoperation controller design is simpler than in many other methods. The only design vectors are $\mathcal{V}_{md}$ and $\mathcal{V}_{sd}$ with scaling parameters κ_p, κ_f and control parameters A, C, Λ.

Remark 5.4: This approach is robust against time delay. However, for applications with large time delay, e.g. 5 to 7 seconds, no motion/force tracking is provided. A local simulator is then required

[2].

Remark 5.5: The results presented in this paper strongly support other works like hand controller design for virtual worlds [29, 30], since transparency is important regardless of real or virtual subjects.

VI Conclusion

In this paper, a novel controller design method has been proposed for unilateral/bilateral teleoperation systems in both position and rate control. The approach guarantees stability, does nt use acceleration measurements, and can be used with arbitrary motion/force scaling. This approach possesses four advantages relative to previous teleoperation controllers. First, its stability is guaranteed and robust against time delays so as to provide a solid basis for achieving good transparency. Within a pre-specified frequency range, the overall master/slave teleoperated system is equivalent to a free-floating mass plus a linear damper specified by control and scaling parameters, which allows asymptotic motion tracking and force tracking. Second, structured system uncertainties are well compensated by applying independent parameter adaptation and strong feedback control. Third, this approach is applicable to both rigid and flexible environments. Fourth, the controller design takes care of the nonlinear dynamics of the robots and incorporates reasonable human operator and rigid/flexible environment models. Benefitting from the use of the *virtual decomposition* approach [21], only the dynamics of rigid links and joints and the dynamics of the environment and the operator are required to construct the dynamics of the master/slave robots. Experiments have shown excellent results in motion tracking and very good results in force tracking. Topics for further research include performance evaluation for doing real-world tasks, development of more accurate operator and environment models, and theoretical analysis addressing the transitions between free and contact motions.

Appendix A

In view of the definitions of $\mathcal{V}_s$, $\mathcal{T}_s$, $\mathcal{M}_s$, $\mathcal{C}_s$, $\mathcal{G}_s$, and (3), (6), (7)-(9), it follows that

$$\begin{aligned} & \mathcal{M}_s\ (\mathcal{T}_s\ \dot{\mathcal{V}}_s + \dot{\mathcal{T}}_s\ \mathcal{V}_s) + \mathcal{C}_s\ \mathcal{T}_s\ \mathcal{V}_s + \mathcal{G}_s \\ = & \begin{bmatrix} I_1^*\ \ddot{q}_1 + \xi_1(t) + d_1 \\ \vdots \\ I_6^*\ \ddot{q}_6 + \xi_6(t) + d_6 \\ M_{L_1}\ \frac{d}{dt}({}^{L_1}V) + C_{L_1}\ {}^{L_1}V + G_{L_1} \\ \vdots \\ M_{L_6}\ \frac{d}{dt}({}^{L_6}V) + C_{L_6}\ {}^{L_6}V + G_{L_6} \\ \sigma_f\ [M_f\ \ddot{\mathcal{X}}_{sf} + D_f\ \dot{\mathcal{X}}_{sf} + \delta\ K_f\ \mathcal{X}_{sf} + (1-\delta)\ \varphi_f] \end{bmatrix} = \begin{bmatrix} \underline{\tau}_1 \\ \vdots \\ \underline{\tau}_6 \\ {}^{L_1}\underline{F} \\ \vdots \\ {}^{L_6}\underline{F} \\ \mathcal{F}_{sf} \end{bmatrix} . \end{aligned} \tag{A1}$$

It follows from (5), (8), (10), and the definition of T_s that

$$\tau_s = T_s \left(\mathcal{T}_s^T \begin{bmatrix} \underline{\tau}_1 \\ \vdots \\ \underline{\tau}_6 \\ {}^{L_1}\underline{F} \\ \vdots \\ {}^{L_6}\underline{F} \\ \mathcal{F}_{sf} \end{bmatrix} + \begin{bmatrix} 0 \\ \sigma_r\ \mathcal{F}_{sr} \end{bmatrix} \right) . \tag{A2}$$

Combining (A1) and (A2) yields (11).

Appendix B

A simple example is taken here to show the block diagram of the control law (16). This is a two dimensional system with point mass M, see Fig. B1(a). The x direction is subject to a flexible constraint characterized by mass m, damping b, and stiffness k. The y direction is subject to a rigid constraint with zero velocity. The control forces are F_x for the x direction and F_y for the y direction. The contact forces from the point mass toward the flexible/rigid environment are f_{cx} and f_{cy}, respectively.

1) Control of x Direction: The dynamics in the x direction can be written as

$$M\ \dot{V}_x + d_x = F_x - f_{cx}\ , \tag{B1}$$

where V_x is the velocity in the x direction, d_x is an unknown constant which has the same role as d_j in (8). Assume that the update gain for $\hat{d}_x$ is particular larger than those for $\hat{M}$, $\hat{m}$, $\hat{b}$, and $\hat{k}$. It follows

from (21) that

$$\hat{d}_x = K_{xI}\int_0^t (V_{xr} - V_x)dt \,, \tag{B2}$$

$$V_{xr} \triangleq V_{xd} - A\tilde{f}_{cx} \,, \tag{B3}$$

where $K_{xI} > 0$, V_{xd} denotes a reference signal. The variable $\tilde{f}_{cx}$ is defined by

$$\tilde{f}_{cx} \triangleq \frac{C}{s+C} f_{cx} \,. \tag{B4}$$

In view of (B2) and (B3), it follows from (16) that

$$\begin{aligned} F_x &= (\hat{M}+\hat{m})\dot{V}_{xr} + \hat{b}V_x + \hat{k}\int_0^t V_x dt + K_{xI}\int_0^t (V_{xr} - V_x)dt + K_x(V_{xr} - V_x) \\ &= (\hat{M}+\hat{m})\dot{V}_{xr} + K_x V_{xr} + K_{xI}\int_0^t V_{xr}dt - [K_x V_x + K_{xI}\int_0^t V_x dt - \hat{b}V_x - \hat{k}\int_0^t V_x dt] \end{aligned} \tag{B5}$$

with $K_x > 0$. From (B3) to (B5), the block diagram of the control system in the x direction is represented by Fig. B1(b) with

$$C_x = K_x + \frac{K_{xI}}{s} - \hat{b} - \frac{\hat{k}}{s} \,, \tag{B6}$$

$$G_b = (\hat{M}+\hat{m})s + K_x + \frac{K_{xI}}{s} \,, \tag{B7}$$

$$G_a = G_b \frac{AC}{s+C} \,. \tag{B8}$$

2) Control System in the y Direction: The dynamics in the y direction can be written as

$$d_y = F_y - f_{cy} \,, \tag{B9}$$

$$V_y = 0 \,, \tag{B10}$$

where d_y denotes an unknown constant and V_y is the velocity. In view of (21), the estimate of d_y results in

$$\hat{d}_y = K_{yI}\int_0^t (V_{yr} - V_y)dt \,, \tag{B11}$$

$$V_{yr} \triangleq V_{yd} - A\tilde{f}_{cy} \,, \tag{B12}$$

where $K_{yI} > 0$, V_{yd} denotes a reference signal. The variable $\tilde{f}_{cy}$ is defined by

$$\tilde{f}_{cy} \triangleq \frac{C}{s+C} f_{cy} \,. \tag{B13}$$

The control law (16) employs

$$
\begin{aligned}
F_y &= \hat{M}\dot{V}_{yr} + K_{yI}\int_0^t (V_{yr} - V_y)dt + F_{yd} + K_y(V_{yr} - V_y) \\
&= \hat{M}\dot{V}_{yr} + K_y V_{yr} + K_{yI}\int_0^t V_{yr}dt + F_{yd}\ , \qquad \text{(B14)} \\
F_{yd} &\triangleq \frac{1}{A}\left(\frac{1}{C}\,\dot{V}_{yd} + V_{yd}\right)\ . \qquad \text{(B15)}
\end{aligned}
$$

The block diagram is illustrated in Fig. B1(c).

References

[1] T. B. Sheridan, "Telerobotics," *Automatica*, vol.25, no.4, pp.487-507, 1989.

[2] G. Hirzinger, B. Brunner, J. Dietrich, and J. Heindl, "Sensor-based space robotics – ROTEX and its telerobotic features," *IEEE Trans. Robotics and Automation*, vol.9, no.5, pp.649-663, 1993.

[3] B. Hannaford, L. Wood, D. A. McAffee, and H. Zak, "Performance evaluation of a six-axis generalized force-reflecting teleoperator," *IEEE Trans. Systems, Man, and Cybernetics*, vol.21, no.3, pp.620-633, 1991.

[4] A. K. Bejczy, "Teleoperators," *IEEE Industrial Electronics Society Newsletter*, pp.4-12, March 1996.

[5] A. A. Goldenberg, J. Wiercienski, P. Kuzan, C. Szymczyk, R. G. Fenton, and B. Shaver, "A remote manipulator for forestry operation," *IEEE Trans. Robotics and Automation*, vol.11, no.2, pp.185-197, 1995.

[6] J. Funda, R. H. Taylor, B. Eldridge, S. Gomory, and K. G. Gruben, "Constrained Cartesian motion control for teleoperated surgical robots," *IEEE Trans. Robotics and Automation*, vol.12, no.3, pp.453-465, 1996.

[7] B. Hannaford, "A design framework for teleoperators with kinesthetic feedback," *IEEE Trans. Robotics and Automation*, vol.5, no.4, pp.426-434, 1989.

[8] K. Kosuge, J. Ishikawa, K. Furuta, and M. Sakai, "Control of single-master multi-slave manipulator system using VIM," *Proc. 1990 IEEE Int. Conf. Robotics and Automation*, pp.1172-1177, 1990.

[9] A. A. Goldenberg, D. Bastas, and Y. Strassberg, "On the bilateral control of master-slave teleoperators," *Robotersysteme*, vol.7, pp.91-99, 1991.

[10] R. J. Anderson and M. W. Spong, "Bilateral control of teleoperators with time delay," *IEEE Trans. Automatic Control*, vol.34, no.5, pp.494-501, 1989.

[11] R. J. Anderson, "Building a modular robot control system using passivity and scattering theory," *Proc. of 1996 IEEE Int. Conf. Robotics and Automation*, pp.698-705, 1996.

[12] R. J. Anderson and M. W. Spong, "Asymptotic stability for force reflecting teleoperators with time delay," *Int. J. Robotics Research*, vol.11, no.2, pp.135-149, 1992.

[13] G. M. H. Leung, B. A. Francis, and J. Apkarian, "Bilateral controller for teleoperators with time delay via μ-synthesis," *IEEE Trans. Robotics and Automation*, vol.11, no.1, pp.105-116, 1995.

[14] D. A. Lawrence, "Stability and transparency in bilateral teleoperation," *IEEE Trans. Robotics and Automation*, vol.9, no.5, pp.624-637, 1993.

[15] Y. Yokokohji and T. Yoshikawa, "Bilateral control of master-slave manipulators for ideal kinesthetic coupling–formulation and experiment," *IEEE Trans. Robotics and Automation*, vol.10, no.5, pp.605-620, 1994.

[16] J. E. Colgate, "Robust impedance shaping telemanipulation," *IEEE Trans. Robotics and Automation*, vol.9, no.4, pp.374-384, 1993.

[17] S. Lee and H. S. Lee, "Modeling, design, and evaluation of advanced teleoperator control systems with short time delay," *IEEE Trans. Robotics and Automation*, vol.9, no.5, pp.607-623, 1993.

[18] H. Kazerooni, T. I. Tsay, and K. Hollerbach, "A controller design framework for telerobotic systems," *IEEE Trans. Control Systems Technology*, vol.1, no.1, pp.50-62, 1993.

[19] J. Yan and S. E. Salcudean, "Teleoperation controller design using H_∞-optimization with application to motion-scaling," *IEEE Trans. Control Systems Technology*, vol.4, no.3, pp.244-258, 1996.

[20] S. E. Salcudean, N. M. Wong, and R. L. Hollis, "Design and control of a force-reflecting teleoperation system with magnetically levitated master and wrist," *IEEE Trans. Robotics and Automation*, vol.11, no.6, pp.844-858, 1995.

[21] W. H. Zhu, Y. G. Xi, Z. J. Zhang, Z. Bien, and J. De Schutter, "Virtual decomposition based control for generalized high dimensional robotic systems with complicated structure," *IEEE Trans. Robotics and Automation*, vol.13, no.3, pp.411-436, 1997.

[22] H. Kazerooni and M. G. Her, "The dynamics and control of a haptic interface device," *IEEE Trans. Robotics and Automation*, vol.10, no.4, pp.453-464, 1994.

[23] J. D. Cooke, "Dependence of human arm movements in limb mechanical properties," *Brain Res.*, vol.165, pp.366-369, 1979.

[24] J. J. E. Slotine and W. P. Li, "Adaptive manipulator control: a case study," *IEEE Trans. Automatic Control*, vol.AC-33, no.11, pp.995-1003, 1988.

[25] Y. H. Liu, S. Arimoto, and K. Kitagaki, "Adaptive control for holonomically constrained robots: time-invariant and time-variant cases," *Proc. 1995 IEEE Int. Conf. Robotics and Automation*, pp.905-912, 1995.

[26] R. R. Y. Zhen and A. A. Goldenberg, "An adaptive approach to constrained robot motion control", *Proc. 1995 IEEE Int. Conf. Robotics Automation*, pp.1833-1838, 1995.

[27] M. Zhu and S. E. Salcudean, "Achieving transparency for teleoperator systems under position and rate control," *Proc. of IROS'95*, 1995.

[28] W. H. Zhu, S. E. Salcudean, and M. Zhu, "Experiments with transparent teleoperation under position and rate control," *Proc. 1999 IEEE Int. Conf. Robotics Automation*, pp.1870-1875, 1999.

[29] S. P. DiMaio, S. E. Salcudean, C. Reboulet, S. Tafazoli, and K. Hashtrudi-Zaad, "A virtual excavator for controller development and evaluation," *Proc. 1998 IEEE Int. Conf. Robotics and Automation*, Leuven, Belgium, 1998.

[30] L. Stocco, S.E. Salcudean, F. Sassani, "Mechanism design for global isotropy with applications to haptic interfaces", *Proceedings of ASME Winter Annual Meeting* (Dallas, Texas), vol.61, pp.115-122, 1997.

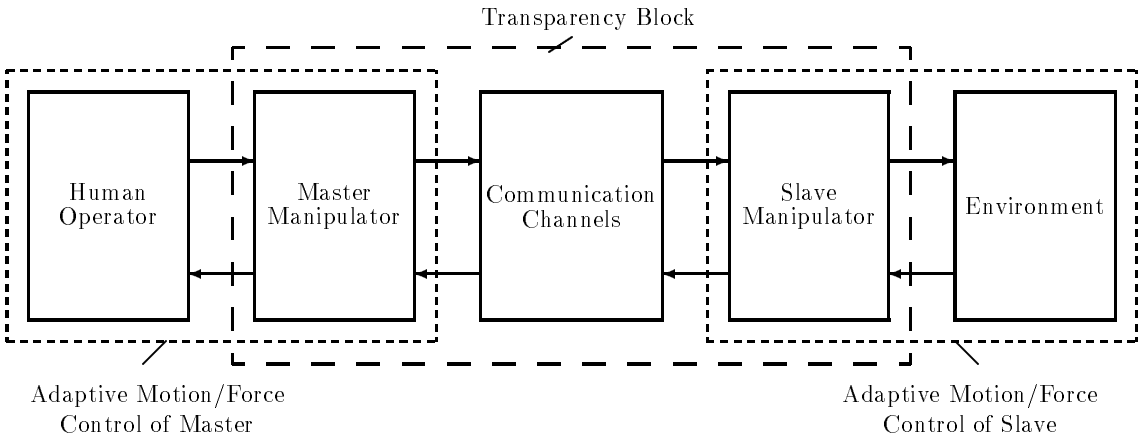

Fig. 1 Stability guaranteed teleoperation control

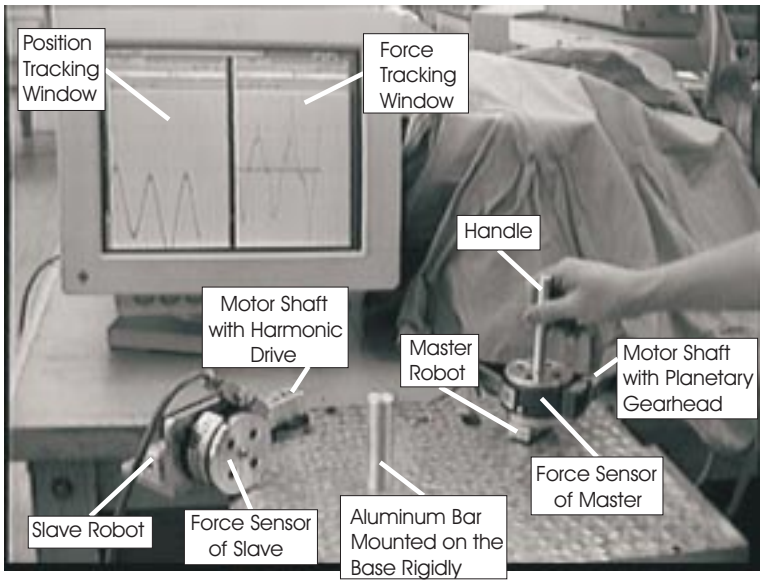

Fig. 3 Experimental set-up

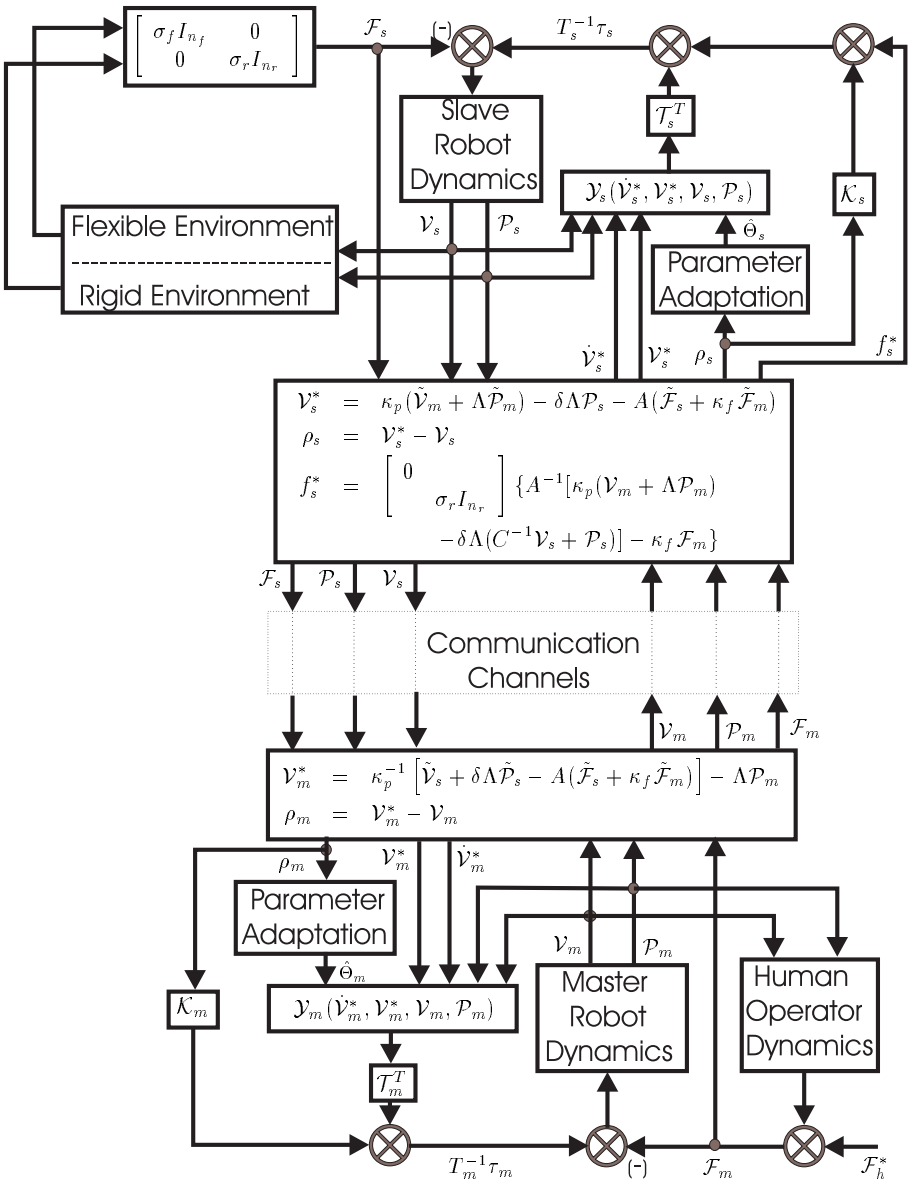

Fig. 2 Diagram of bilateral teleoperation control system

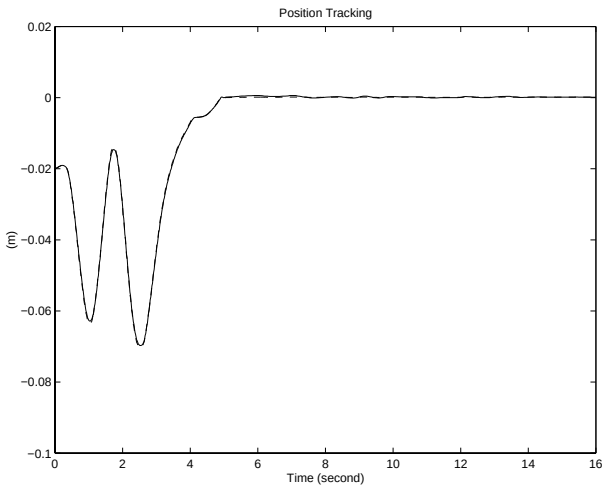

Fig.4 (a)

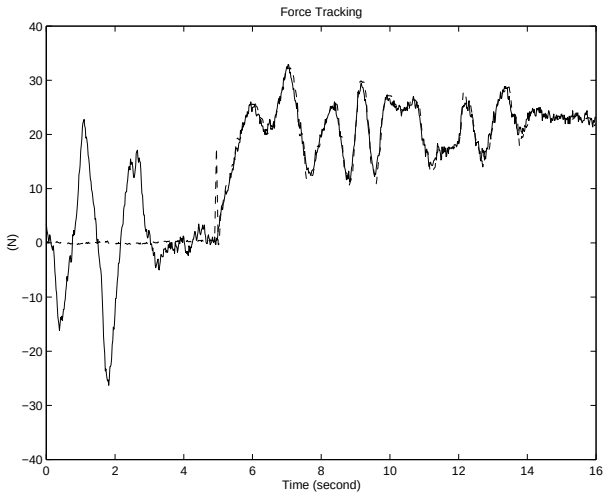

Fig.4 (b)

Fig. 4 Position-force control with $\kappa_p = 1.0$, $\kappa_f = 10.0$ for rigid contact

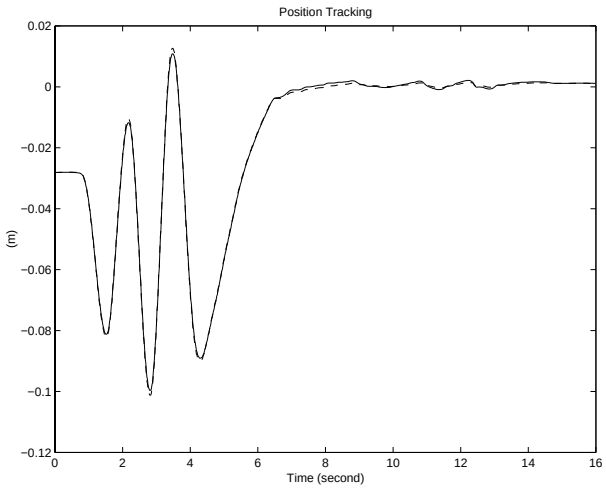

Fig.5 (a)

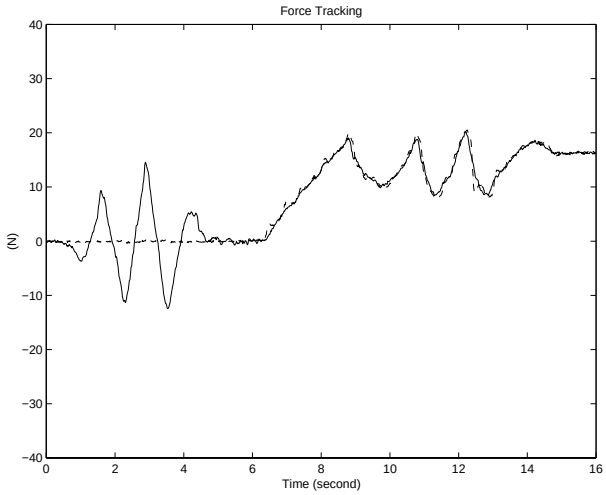

Fig.5 (b)

Fig. 5 Position-force control with $\kappa_p = 1.0$, $\kappa_f = 2.0$ for flexible contact

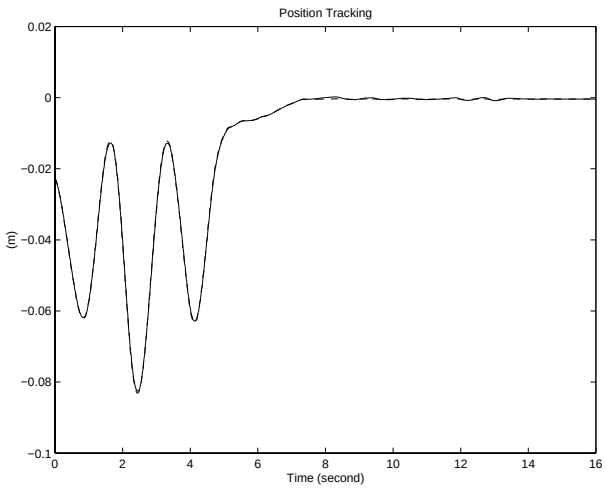

Fig.6 (a)

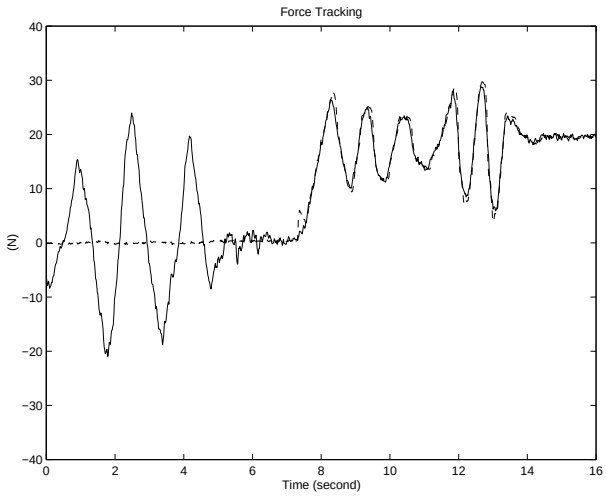

Fig.6 (b)

Fig. 6 Position-force control with $\kappa_p = 0.5$, $\kappa_f = 5.0$ for rigid contact

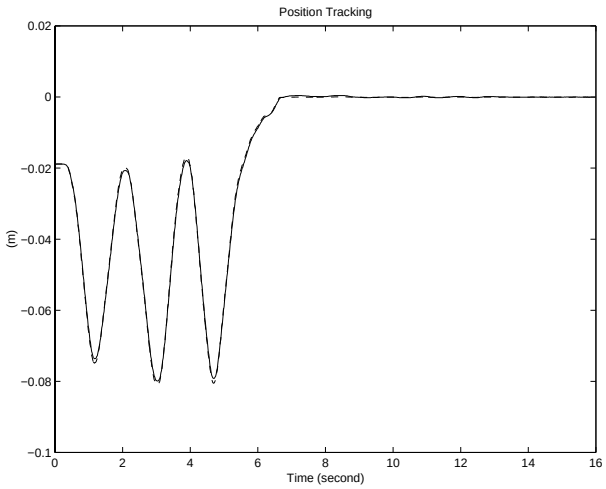

Fig.7 (a)

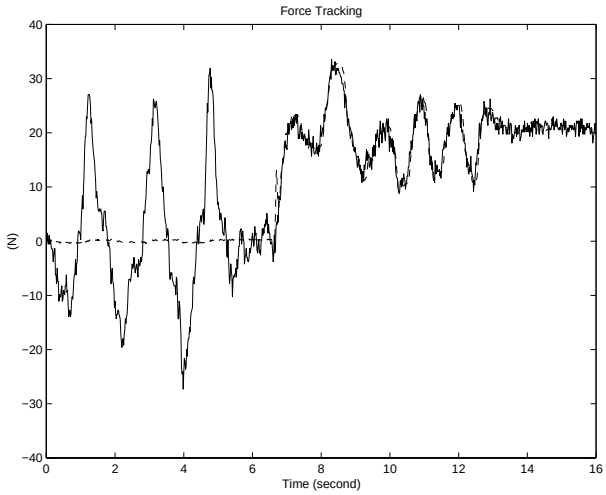

Fig.7 (b)

Fig. 7 Position-force control with $\kappa_p = 2.0$, $\kappa_f = 20.0$ for rigid contact

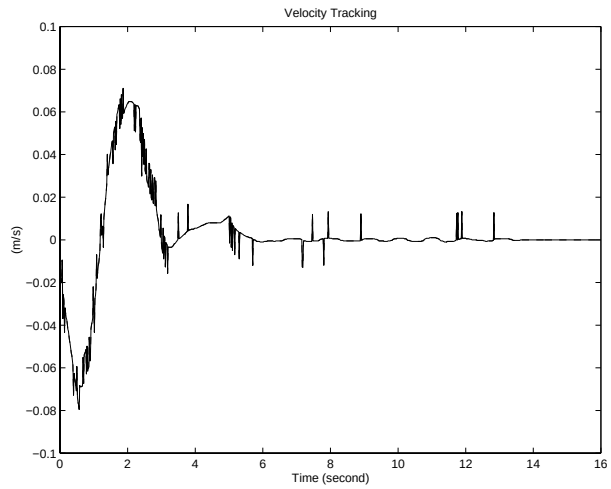

Fig.8 (a)

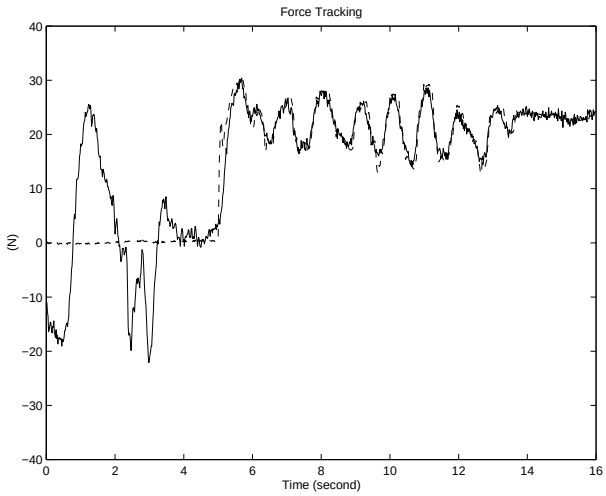

Fig.8 (b)

Fig. 8 Rate-force control type 1 with $\kappa_p = 1.0$, $\Lambda = 10.0$, $\kappa_f = 10.0$ for rigid contact

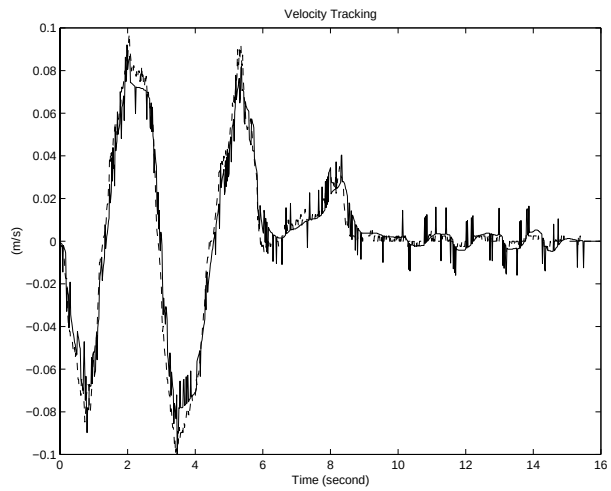

Fig.9 (a)

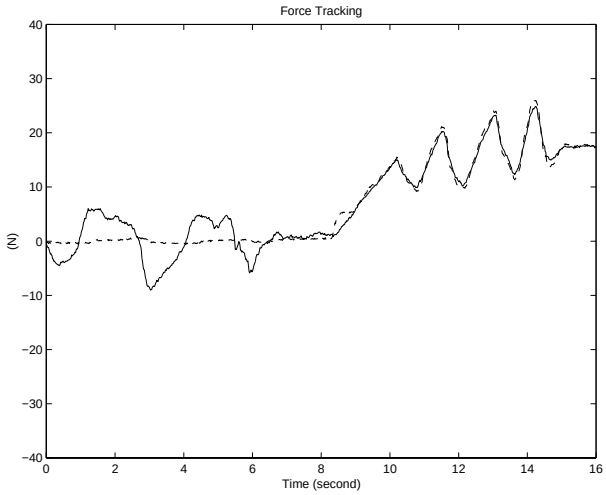

Fig.9 (b)

Fig. 9 Rate-force control type 1 with $\kappa_p = 1.0$, $\Lambda = 10.0$, $\kappa_f = 2.0$ for flexible contact

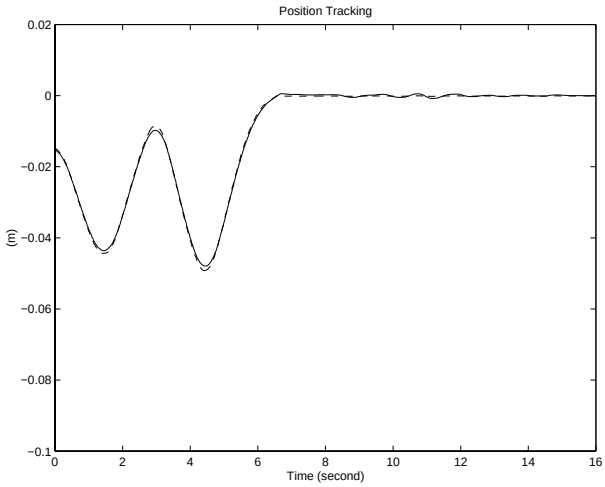

Fig.10 (a)

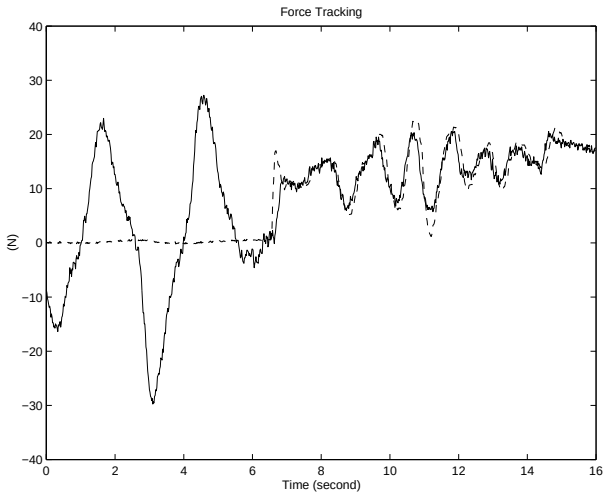

Fig.10 (b)

Fig. 10 Position-force control with 0.1s one-way time delay ($\kappa_p = 1.0$, $\kappa_f = 10.0$)

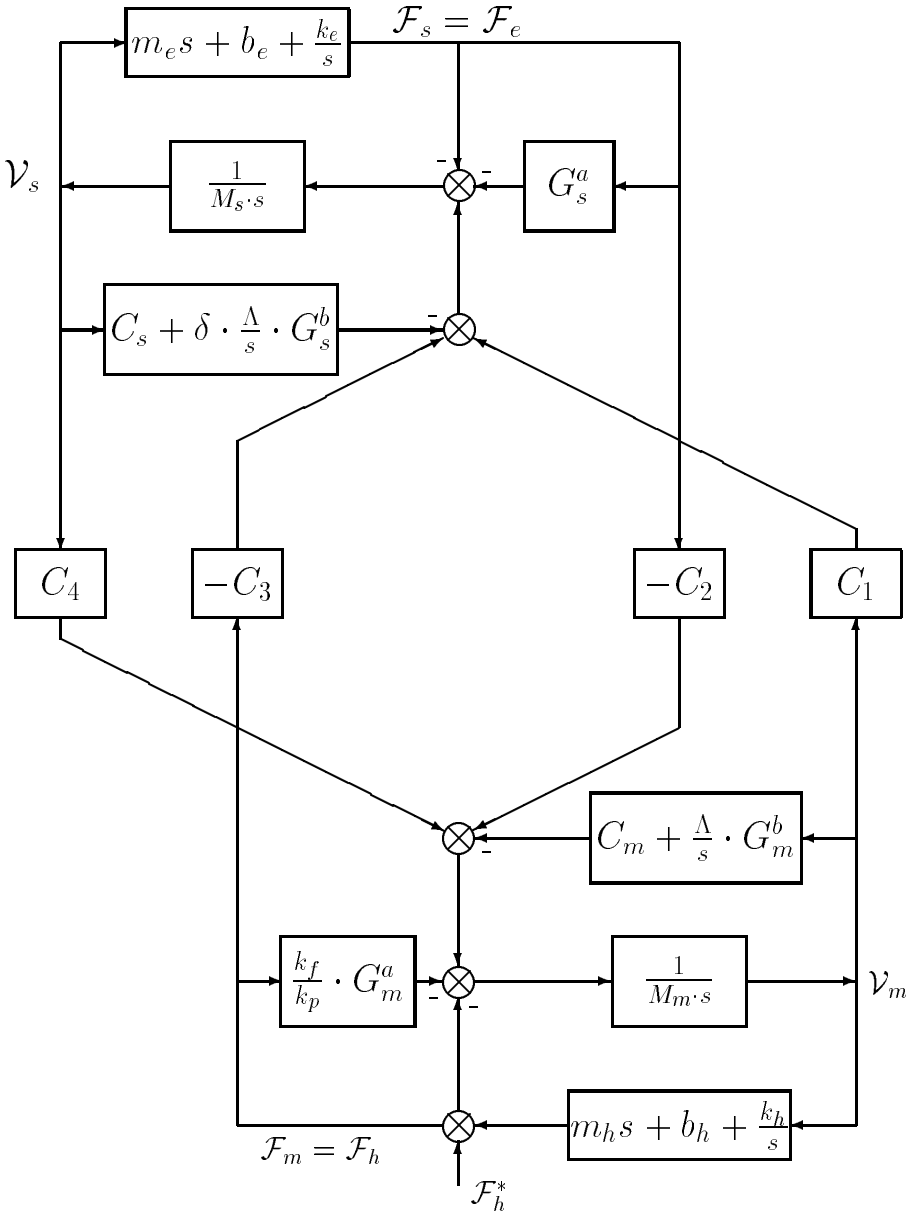

Fig. 11 Block diagram of an 1-DOF teleoperation system

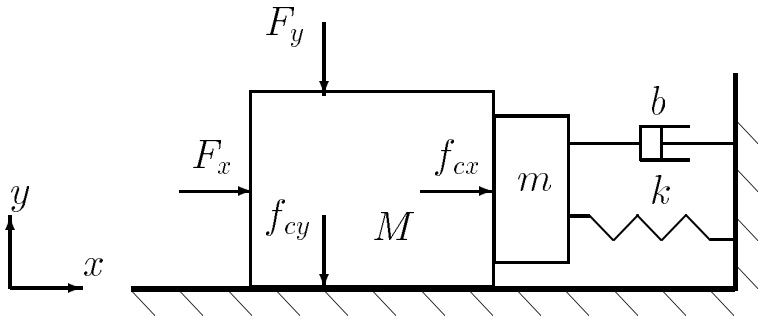

Fig. B1(a)

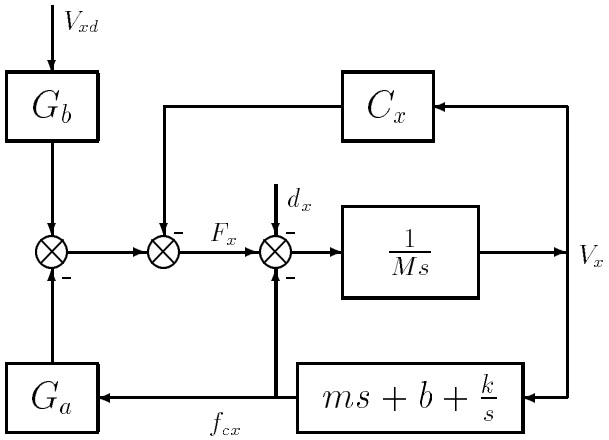

Fig. B1(b)

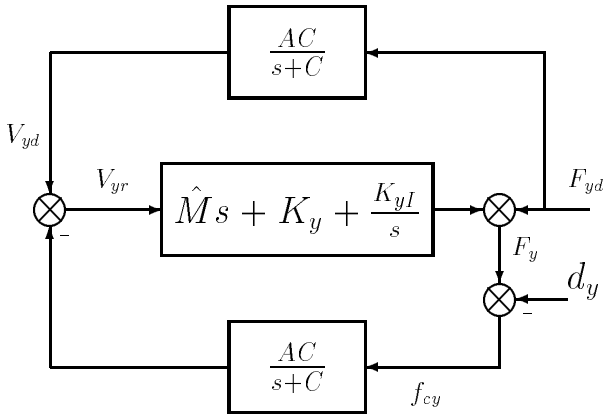

Fig. B1(c)

Fig. B1 A two-DOF motion/force control system with flexible/rigid constraints